



HAL
open science

Bayesian Calibration of the Mg/Ca Paleothermometer in Planktic Foraminifera

Jessica E. Tierney, Steven B. Malevich, William Gray, Lael Vetter, Kaustubh
J Thirumalai

► **To cite this version:**

Jessica E. Tierney, Steven B. Malevich, William Gray, Lael Vetter, Kaustubh J Thirumalai. Bayesian Calibration of the Mg/Ca Paleothermometer in Planktic Foraminifera. *Paleoceanography and Paleoclimatology*, 2019, 34 (12), pp.2005-2030. 10.1029/2019PA003744 . hal-02973694

HAL Id: hal-02973694

<https://hal.science/hal-02973694>

Submitted on 28 Oct 2020

HAL is a multi-disciplinary open access archive for the deposit and dissemination of scientific research documents, whether they are published or not. The documents may come from teaching and research institutions in France or abroad, or from public or private research centers.

L'archive ouverte pluridisciplinaire **HAL**, est destinée au dépôt et à la diffusion de documents scientifiques de niveau recherche, publiés ou non, émanant des établissements d'enseignement et de recherche français ou étrangers, des laboratoires publics ou privés.

Paleoceanography and Paleoclimatology

RESEARCH ARTICLE

10.1029/2019PA003744

Key Points:

- We introduce Mg/Ca Bayesian calibrations for planktic foraminifera
- Hierarchical modeling is used to constrain multivariate Mg/Ca sensitivities
- For deep-time applications, we incorporate estimates of Mg/Ca of seawater

Supporting Information:

- Supporting Information S1
- Data Set S1
- Data Set S2
- Data Set S3
- Data Set S4
- Data Set S5

Correspondence to:

J. E. Tierney,
jesst@email.arizona.edu

Citation:

Tierney, J. E., Malevich, S. B., Gray, W., Vetter, L., & Thirumalai, K. (2019). Bayesian calibration of the Mg/Ca paleothermometer in planktic foraminifera. *Paleoceanography and Paleoclimatology*, 34, 2005–2030. <https://doi.org/10.1029/2019PA003744>





Received 1 AUG 2019

Accepted 31 OCT 2019

Accepted article online 12 NOV 2019

Published online 13 DEC 2019

Bayesian Calibration of the Mg/Ca Paleothermometer in Planktic Foraminifera

Jessica E. Tierney¹ , Steven B. Malevich¹ , William Gray² , Lael Vetter¹, and Kaustubh Thirumalai¹ 

¹Department of Geosciences, University of Arizona, Tucson, AZ, USA, ²Laboratoire des Sciences du Climat et de l'Environnement (LSCE/IPSL), Gif-sur-Yvette, France

Abstract The Mg/Ca ratio of planktic foraminifera is a widely used proxy for sea-surface temperature but is also sensitive to other environmental factors. Previous work has relied on correcting Mg/Ca for nonthermal influences. Here, we develop a set of Bayesian models for Mg/Ca in four major planktic groups—*Globigerinoides ruber* (including both pink and white chromotypes), *Trilobatus sacculifer*, *Globigerina bulloides*, and *Neogloboquadrina pachyderma* (including *N. incompta*)—that account for the multivariate influences on this proxy in an integrated framework. We use a hierarchical model design that leverages information from both laboratory culture studies and globally distributed core top data, allowing us to include environmental sensitivities that are poorly constrained by core top observations alone. For applications over longer geological timescales, we develop a version of the model that incorporates changes in the Mg/Ca ratio of seawater. We test our models—collectively referred to as BAYMAG—on sediment trap data and on representative paleoclimate time series and demonstrate good agreement with observations and independent sea-surface temperature proxies. BAYMAG provides probabilistic estimates of past temperatures that can accommodate uncertainties in other environmental influences, enhancing our ability to interpret signals encoded in Mg/Ca.

Plain Language Summary The amount of magnesium (Mg) incorporated into the calcite shells of tiny protists called foraminifera is determined by the temperature of the water in which they grew. This allows paleoclimatologists to measure the magnesium-to-calcium (Mg/Ca) ratio of fossil foraminiferal shells and determine how past sea-surface temperatures have changed. However, other factors can influence Mg/Ca, like the salinity and pH of seawater. Here, we develop Bayesian models of foraminiferal Mg/Ca that account for all of the influences on Mg/Ca and show how we can use these to improve our interpretations of Mg/Ca data.

1. Introduction

The magnesium-to-calcium (Mg/Ca) ratio of planktic foraminifera is a commonly used proxy method for reconstructing past sea-surface temperatures (SSTs). It has played a pivotal role informing our understanding of tropical climate dynamics in the Late Quaternary (Lea et al., 2000, 2003; Rosenthal et al., 2003; Stott et al., 2007) as well as in deeper geologic time (e.g., Evans et al., 2018). The proxy has theoretical basis in thermodynamics, which predicts a nonlinear increase in Mg incorporation into calcite as temperatures rise (Oomori et al., 1987). Laboratory culturing of planktic foraminifera confirms an exponential dependence of Mg/Ca on temperature, albeit with a stronger sensitivity than thermodynamic predictions, indicating that biological “vital effects” also play a role (Lea et al., 1999; Nürnberg et al., 1996). Laboratory experiments also demonstrate that Mg/Ca in foraminifera is sensitive to other environmental factors, such as salinity and pH (Evans, Wade, et al., 2016; Dueñas-Bohórquez et al., 2009; Hönisch et al., 2013; Kisakürek et al., 2008; Lea et al., 1999). The extent to which these secondary factors compromise SST prediction from Mg/Ca is an ongoing topic of investigation (Arbuszewski et al., 2010; Evans, Wade, et al., 2016; Ferguson et al., 2008; Gray & Evans, 2019; Gray et al., 2018; Hönisch et al., 2013; Mathien-Blard & Bassinot, 2009). Beyond competing environmental factors, the depositional environment also influences Mg/Ca. If the calcite saturation state of the bottom waters is low, partial dissolution of foraminiferal calcite occurs, lowering Mg/Ca (Brown & Elderfield, 1996; Regenberg et al., 2006, 2014; Rosenthal et al., 2000).

Previous calibrations for Mg/Ca have been based on laboratory culturing experiments (Gray & Evans, 2019; Lea et al., 1999; Nürnberg et al., 1996), sediment trap data (Anand et al., 2003; Gray et al., 2018), or modern core tops (Dekens et al., 2002; Elderfield & Ganssen, 2000; Khider et al., 2015; Saenger & Evans, 2019). Culture experiments provide precise constraints on environmental sensitivities but are limited in that laboratory conditions are not perfect analogs for the natural environment. Sediment traps have an advantage in that seasonality of foraminiferal occurrence and corresponding ocean temperatures are well constrained, but they do not account for the effects of dissolution or bioturbation. Sedimentary core tops integrate effects associated with both occurrence and preservation and are thus better analogs for the conditions typical of the geological record, but uncertainties in seasonal preferences and the depth of calcification can in some cases lead to misleading inference of secondary environmental sensitivities (Hertzberg & Schmidt, 2013; Hönisch et al., 2013).

Here, we use both core top and laboratory culture data to develop a suite of Bayesian hierarchical models for Mg/Ca. We collate over 1,000 sedimentary Mg/Ca measurements to formulate new calibrations for four major planktic groups: *Globigerinoides ruber* (including both pink and white chromotypes), *Trilobatus sacculifer*, *Globigerina bulloides*, and *Neogloboquadrina pachyderma* (including *N. incompta*). First, we assess the impact of adding known secondary environmental predictors (bottom water saturation state, salinity, pH, and laboratory cleaning technique) to a Mg/Ca calibration model. We then compute both pooled (all species groups considered together) and hierarchical (species groups considered separately) calibration models using Bayesian methodology similar to that previously developed for core top models of planktic foraminiferal $\delta^{18}\text{O}$ (Malevich et al., 2019). We assess the validity of the new regressions by applying them to sediment trap data and downcore measurements of foraminiferal Mg/Ca. Given that planktic foraminiferal Mg/Ca is increasingly used for SST estimation in deeper geological time, we develop a version of our model that accounts for secular changes in the Mg/Ca composition of seawater. The overarching goal of this study is to develop a flexible set of forward and inverse models for planktic foraminiferal Mg/Ca that estimate observational uncertainties and can be used in a variety of paleoclimatic applications, including interproxy comparisons, proxy-model comparisons, and data assimilation.

2. Data Compilation

We compiled 1,279 core top Mg/Ca measurements from the literature (Aagaard-Sørensen et al., 2014; Arbuszewski et al., 2013; Barker et al., 2005; Benway et al., 2006; Boussetta et al., 2012; Brown & Elderfield, 1996; Cléroux et al., 2008; Dahl & Oppo, 2006; Dai et al., 2019; de Garidel-Thoron et al., 2007; Dekens et al., 2002; Dyez et al., 2014; Elderfield & Ganssen, 2000; Fallet et al., 2012; Farmer et al., 2005; Ferguson et al., 2008; Ganssen & Kroon, 2000; Gebregiorgis et al., 2016; Gibbons et al., 2014; Hastings et al., 1998; Hollstein et al., 2017; Johnstone et al., 2011; Keigwin et al., 2005; Khider et al., 2015; Kozdon et al., 2009; Kristjánssdóttir et al., 2017; Kubota et al., 2010; Lea et al., 2003, 2006; Leduc et al., 2007; Levi et al., 2007; Linsley et al., 2010; Marchitto et al., 2010; Mashiotto et al., 1999; Mathien-Blard & Bassinot, 2009; Meland et al., 2006; Moffa-Sánchez et al., 2014; Mohtadi et al., 2010, 2011; Morley et al., 2017; Nürnberg et al., 2008; Oppo et al., 2009; Oppo & Sun, 2005; Pahnke et al., 2003; Palmer & Pearson, 2003; Parker et al., 2016; Regenberg et al., 2006, 2009; Richey et al., 2007, 2009; Riethdorf et al., 2013; Romahn et al., 2014; Rosenthal et al., 2003; Rosenthal & Boyle, 1993; Russell et al., 1994; Rustic et al., 2015; Sabbatini et al., 2011; Saraswat et al., 2013; Schmidt et al., 2004; Schmidt, Chang, et al., 2012; Schmidt, Weinlein et al., 2012; Steinke et al., 2005; Steinke et al., 2008; Stott et al., 2007; Sun et al., 2005; Thornalley et al., 2011; Tierney et al., 2016; van Raden et al., 2011; Vázquez Riveiros et al., 2016; Visser et al., 2003; Wei et al., 2007; Weldeab et al., 2005, 2006, 2007, 2014; Xu et al., 2010; Yu et al., 2008). The data collection includes the core name, the site location (latitude, longitude, and water depth), the interval of the core sampled (if provided), the Mg/Ca ratio, corresponding $\delta^{18}\text{O}$ and $\delta^{13}\text{C}$ measurements (if provided), the species, the size fraction sampled (if provided), and the source reference. Since previous work points to a systematic offset in Mg/Ca based on the cleaning method used in the laboratory (Khider et al., 2015; Rosenthal et al., 2004), we flagged the data according to the type of cleaning performed, with a value of 0 assigned to samples cleaned without a reductive step (e.g., Barker et al., 2003) and a value of 1 assigned to samples cleaned with the reductive step (e.g., Boyle & Keigwin, 1985). We assigned a quality control flag to each core top—indicating whether the data should be included in our calibration model or not—based on the interpretation of the data in the original study. For example, data that were noted as suspect due to small sample size or encrustation of high-Mg coatings were

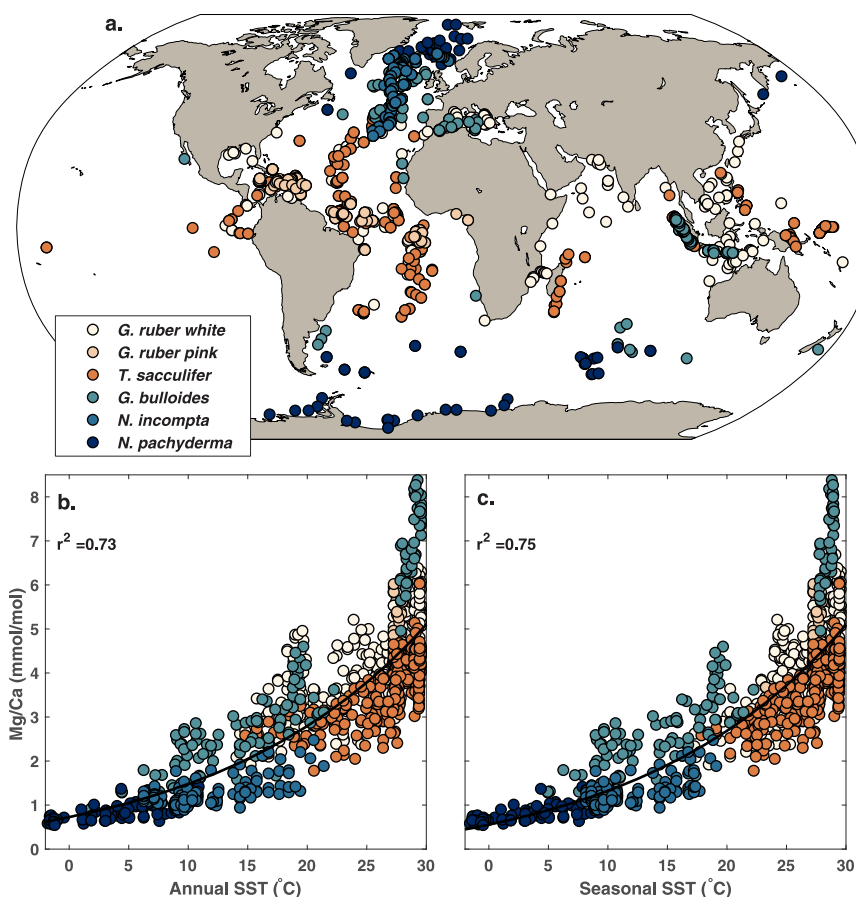


Figure 1. (a) Geographical distribution of the Mg/Ca core top data, with an “include” flag of 1 ($N = 1,182$), by species. (b) The relationship between Mg/Ca and mean annual SSTs. (c) The relationship between Mg/Ca and estimated seasonal SSTs. Black lines through the data in (b) and (c) represent the best fit exponential regressions, with r^2 values listed in the upper left.

excluded. We also excluded data from the eastern Mediterranean, where authigenic high-Mg coatings are commonly observed and result in anomalous Mg/Ca values (Sabbatini et al., 2011). This initial quality screen reduced our data set to 1,182 samples, with 452 core tops for *G. ruber white*, 74 for *G. ruber pink*, 292 for *T. sacculifer*, 72 for *N. pachyderma*, 158 for *N. incompta*, and 134 for *G. bulloides* (Figure 1). *G. ruber white* and pink core top samples were subsequently combined and averaged and collectively treated as the *G. ruber* group, recognizing that these chromotypes are closely related genetically (Aurahs et al., 2011) and have similar geochemistry (Richey et al., 2012, 2019). In addition, initial exploration indicated that the *G. ruber pink* data set spanned a limited geographical (tropical-subtropical Atlantic) and temperature ($25\text{--}28^\circ\text{C}$) range, complicating accurate determination of regression coefficients. Likewise, *N. pachyderma* and *N. incompta* were combined and calibrated together as the *N. pachyderma* group. Originally considered to be morphotypes, *N. pachyderma* and *N. incompta* are now classified as genetically different species (Darling et al., 2006) and have different temperature optima (which is accounted for in our seasonal calibration). However, they have similar habitat preferences, living seasonally in the high latitudes in the mixed layer (Darling et al., 2006), and as with *G. ruber pink*, we found that the limited number of *N. pachyderma* core tops challenged calibration in isolation.

The core top data are matched to the nearest gridpoint from the World Ocean Atlas 2013 (WOA13) version 2 (Boyer et al., 2013), from which we draw mean annual and seasonal SSTs and sea-surface salinity (SSS). As with our previous calibration models for foraminiferal $\delta^{18}\text{O}$ (Malevich et al., 2019), we do not explicitly consider depth habitat for the different planktic groups. Although regressing against environmental parameters at 0 m water depth might not be optimal to derive the “true” sensitivities of Mg/Ca, we assume

Table 1

Sea-Surface Temperature Ranges Associated With Peak Abundances for Each Foraminiferal Species Investigated in This Study, Based on Kernel Density Estimates of Shell Fluxes From a Collection of Global Sediment Traps (from Malevich et al., 2019)

Species	Peak abundance SST ranges (° C)		
	Min	Max	Median
<i>G. ruber</i>	22.5	31.9	27.4
<i>T. sacculifer</i>	20.2	30.6	27.0
<i>G. bulloides</i>	3.6	29.2	18.0
<i>N. pachyderma</i>	−0.9	15.3	5.4
<i>N. incompta</i>	6.7	21.1	15.3

that users want to infer past SSTs from mixed-layer species, rather than a calcification depth temperature. In addition, depth preferences tend to covary with seasonal preferences, and so accounting for both can lead to overfitting. We tested this assumption by running our Bayesian calibration models using integrated 0–50 m values; we obtained nearly identical coefficients (not shown). We note that any prescribed depth habitat in a calibration—whether it be 0 or 0–50 m—assumes that it is static in time. Circumventing this assumption requires modeling depth habitat explicitly as a function of thermal tolerance, light, and nutrients (e.g., Lombard et al., 2011). This adds considerable complexity, and paleoclimate applications would require biogeochemical constraints; thus, we leave this for future work.

Seasonal averages are computed using spatially varying estimates of when the peak abundance of each foraminiferal species occurs, according to their individual thermal tolerances. As described in Malevich et al. (2019), these are based on kernel density estimates (KDEs) of sediment trap data (Zarić et al., 2005) and the seasonal cycle in temperature at each site, as inferred from WOA13. For example, the KDE of *G. ruber* abundance indicates that this species prefers SSTs between 22.5 and 31.9 ° C. Thus, for locations with SSTs that seasonally drop below 22.5 ° C, *G. ruber* is assumed to not calcify during those months, and the average seasonal SST would be the mean value for all months above 22.5 ° C. Effectively, this assumes that *G. ruber* Mg/Ca reflects mean annual SSTs at most tropical locations, but warm-season SSTs in the subtropics. We also draw seasonal optima for *N. pachyderma* and *N. incompta* separately, recognizing the distinct temperature preferences of these two species, even though they are ultimately calibrated together. Table 1 lists the minimum, maximum, and median SST preferences for each species according to the KDE method. For *G. ruber*, *T. sacculifer*, and *N. incompta*, our inferred optimal SST ranges are very similar to those modeled by Lombard et al. (2009) from culture data (21–30 ° C, 19–31 ° C, and 6–20 ° C, respectively). Our ranges for *G. bulloides* and *N. pachyderma* are slightly larger (Table 1) than the Lombard et al. (2009) estimates (10–25 ° C and 0–10 ° C, respectively) because the sediment trap data indicate a wider thermal range for these species.

Core tops that fall within the same gridpoint, and contain the same species, are further averaged prior to calibration exercises to reduce the impact of spatial clustering on the regression parameters. This results in an effective core top N of 710 for our regression models, with $N = 307$ for *G. ruber*, $N = 184$ for *T. sacculifer*, $N = 100$ for *G. bulloides* model, and $N = 119$ for *N. pachyderma*.

Since previous work indicates that the carbonate system influences foraminiferal Mg/Ca, we also collate surface water pH and bottom water calcite saturation state (Ω) values for each core site from the Global Ocean Data Analysis Project (GLODAP) version 2 gridded climatology (Lauvset et al., 2016). GLODAPv2 lacks coverage in the Gulf of Mexico, so for core tops in this location, we rely on bottle data collected as part of the second Gulf of Mexico and East Coast Carbon Cruise (GOMECC-2) in 2012 (data publicly available from <http://www.aoml.noaa.gov/ocd/gcc/GOMECC2>) and use the MATLAB implementation of CO2SYS (v1.1, Van Heuven et al., 2011) to compute pH and calcite Ω from measured values of alkalinity, dissolved inorganic carbon, salinity, temperature, pressure, silicate, and phosphate. We used the Mehrbach K1 and K2 constants, as refit by Dickson and Millero (1987).

Overall, our core top data set spans a wide range of SSTs (-1.8 to 29.6°C ; 95% CI = 3.1 to 29.4°C) and Ω (0.7 to 5.5 ; 95% CI = 0.9 to 3.3). Although high and low SSS values are represented in the data set (28.4 to 38.6 psu), the distribution of the data is more restricted (95% CI = 33.3 to 37.5 psu). The range of surface water pH values sampled is limited (7.97 to 8.22 ; 95% CI = 8.02 to 8.17), reflecting the fact that the pH of the modern surface ocean does not have a large dynamic range.

As described below, we also use Mg/Ca data from cultured foraminifera to constrain sensitivities to environmental parameters. We use the compilation of Gray and Evans (2019), with the addition of the *G. ruber* pink data from Allen et al. (2016) and *N. incompta* data from Von Langen et al. (2005) and Davis et al. (2017). This updated culture data set includes 30 *G. ruber* observations, 20 *T. sacculifer* observations, 12 *G. bulloides* observations, 29 *O. universa* observations, and 12 *N. incompta* observations for a total of 103 data points.

3. Model Form and Exploration of Environmental Predictors

Temperature clearly exerts a strong, nonlinear control on core top Mg/Ca, explaining about 75% of the variance in the data (Figures 1b and 1c), in agreement with experimental evidence (e.g., Lea et al., 1999). However, laboratory studies and previous core top investigations have shown that pH, salinity, the saturation state (Ω) at the core site, the cleaning method, and shell size also influence Mg/Ca. Mg/Ca sensitivities to salinity and pH are also considered exponential (Evans, Wade, et al., 2016; Gray et al., 2018; Hönisch et al., 2013; Kisakürek et al., 2008; Lea et al., 1999). Culture experiments suggest a pH sensitivity of -50% to -90% per pH units for *O. universa*, *G. bulloides*, and *G. ruber* (white) (Evans, Brierley, et al., 2016; Gray & Evans, 2019; Lea et al., 1999; Russell et al., 2004; Kisakürek et al., 2008), and Gray et al. (2018) detected a pH sensitivity of a similar magnitude of $-80 \pm 70\%$ (2σ) per pH units in a global compilation of *G. ruber* (white) sediment trap data. However, pH does not seem to impact Mg/Ca in cultures of *N. pachyderma*, *N. incompta* (Davis et al., 2017), and *T. sacculifer* (Allen et al., 2016). Laboratory experiments indicate a moderate sensitivity of planktic Mg/Ca to salinity ($3\text{--}5\%$ per psu) (Allen et al., 2016; Gray & Evans, 2019; Hönisch et al., 2013; Kisakürek et al., 2008; Lea et al., 1999). Previous core top studies suggested a much larger sensitivity ($15\text{--}59\%$, Arbuszewski et al., 2010; Ferguson et al., 2008; Mathien-Blard & Bassinot, 2009), but reanalyses indicated that these high estimates are due either to environmental covariates (Hertzberg & Schmidt, 2013; Hönisch et al., 2013; Khider et al., 2015) or to analytical issues (Dai et al., 2019). Core top observations also reveal a systematic decline in sedimentary planktic Mg/Ca—regardless of species—under low bottom water Ω at the site of deposition (Regenberg et al., 2014). Finally, intralaboratory and interlaboratory comparisons (Barker et al., 2003; Rosenthal et al., 2004) as well as a regression analysis of *G. ruber* (white) core tops (Khider et al., 2015) indicate a systematic offset in measured Mg/Ca of $\sim 10\text{--}15\%$ based on whether the laboratory cleaning method includes a reductive step. Mg/Ca also varies by shell size (Elderfield et al., 2002; Friedrich et al., 2012), but researchers tend to mitigate this effect by picking foraminifera from a restricted size fraction. Preliminary investigations revealed that shell size was not a significant predictor for core top Mg/Ca, so it is not included in our models.

Since temperature, salinity, and pH sensitivities are exponential, we transform Mg/Ca to $\ln(\text{Mg/Ca})$ for model fitting. This transformation also assumes that the errors for a Mg/Ca model follow an exponential distribution; the data in Figures 1b and 1c suggest that this is a valid assumption, as variance increases nonlinearly with temperature. Following Khider et al. (2015), the cleaning parameter acts as a multiplicative term in Mg/Ca space, and thus an additive term in $\ln(\text{Mg/Ca})$ space, with the understanding that reductive cleaning (a value of 1) results in a systematic decline in Mg/Ca. The form of the Mg/Ca dependency on Ω is less clear. Regenberg et al. (2014) and Khider et al. (2015) assume that bottom water saturation impacts Mg/Ca of tests linearly below a certain threshold, which they define based on ΔCO_3^{2-} instead of Ω . These two quantities are functionally equivalent, but we prefer using Ω because it is always a positive value. However, it might be expected, based on reaction kinetics, that Mg/Ca should have a nonlinear dependency on saturation state, with dissolution increasing as saturation state drops (Sjöberg, 1976). Indeed, if we remove the impact of SST on our pooled data set, we find that $\ln(\text{Mg/Ca})$ residuals trend nonlinearly with Ω , with the slope becoming steeper as Ω becomes smaller (Figure 2). The relationship is strongest below an Ω of ~ 1.5 (Figure 2), which is consistent with the ΔCO_3^{2-} threshold of $\sim 40\ \mu\text{mol/kg}$ identified by Regenberg et al. (2014). Ω sensitivity can be approximated by a power function, with a coefficient of -2 (Figure 2). This supports a transformation of Ω to Ω^{-2} in order to linearize the sensitivity of $\ln(\text{Mg/Ca})$ to saturation state.

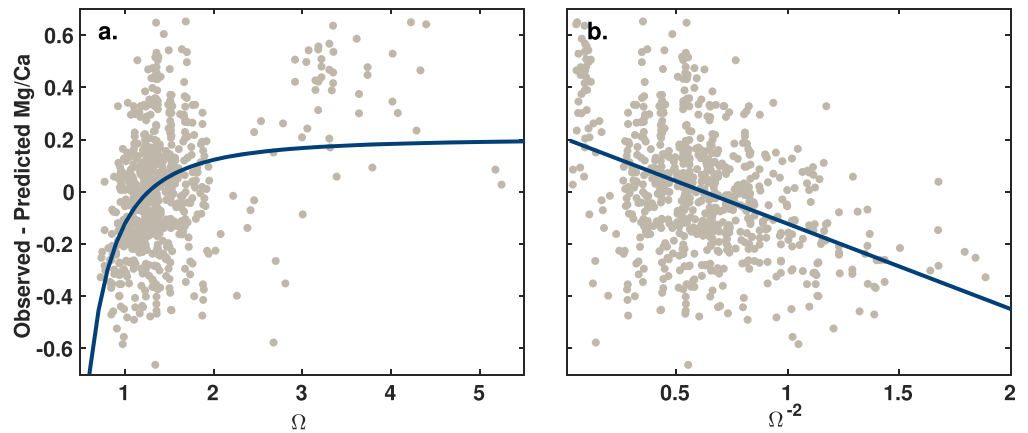


Figure 2. The relationship of core top $\ln(\text{Mg}/\text{Ca})$ residuals (observed-predicted; all species; $N = 710$) to (a) bottom water calcite Ω and (b) Ω^{-2} after removing the dependence on temperature. Dots represent individual core tops; lines show the best fit regression.

The final form of a core top Mg/Ca forward model, based on the physical expectations outlined above, is

$$\ln(\text{Mg}/\text{Ca}) = \alpha + T \cdot \beta_T + S \cdot \beta_S + \text{pH} \cdot \beta_p + \Omega^{-2} \cdot \beta_O + (1 - \text{clean}) \cdot \beta_C + \epsilon, \quad (1)$$

$$\epsilon \sim \mathcal{N}(\mathbf{0}, \sigma^2),$$

where ϵ is the vector of residual errors, approximated by a normal distribution with mean zero and variance σ^2 .

To assess the impact of each environmental variable on model performance, we iteratively computed regressions using ordinary least squares, adding each predictor sequentially. We then compared the Bayesian information criterion (BIC) for each iterative model to determine whether the additional predictor resulted in improvement. The BIC is a criterion for model selection that helps guard against overfitting by penalizing the addition of parameters that do not improve the model fit; lower values (regardless of sign) indicate a better fit. We also analyzed the significance of each predictor's coefficient. We do this for both the pooled data set (using annual and seasonal SST and SSS estimates) and the four species groups (using seasonal SST and SSS estimates) and discuss the results for each predictor in turn.

3.1. Temperature

For both the pooled annual and pooled seasonal data sets, we find that SST alone explains over 80% of the variance in $\ln(\text{Mg}/\text{Ca})$ (Table 2). This is slightly greater than an exponential model for Mg/Ca (Figures 1b and 1c), reflecting some improvement in the fit associated with the assumption that variance increases exponentially. Temperature remains the most important parameter for the individual species models, although it explains only ca. 50% of the variance for the warm-water groups (*G. ruber* and *T. sacculifer*; Table 2). This is due to the relatively restricted temperature ranges for *G. ruber* and *T. sacculifer* (ca. 12° C) compared to those for *G. bulloides* and *N. pachyderma* (>20° C), which allows for more variance to be explained by the other environmental factors. The temperature sensitivity is similar across all species, between 5% and 7% (Table 2). This agrees well with recent reassessments from culture and sediment traps, both of which indicate a temperature sensitivity of ca. 6% (Gray et al., 2018; Gray & Evans, 2019) rather than 9%, as previously assumed (e.g., Anand et al., 2003; Dekens et al., 2002; Khider et al., 2015).

3.2. Bottom Water Calcite Saturation (Ω)

The addition of Ω as a predictor improves almost all of the models (r^2 increases, root mean square error (RMSE) decreases, and BIC decreases), with the biggest impact on the warm-water species (Table 2). The large drop in BIC associated with the addition of this parameter (to the pooled models in particular, where it is about 100) supports long-standing theory and intuition that inclusion of Ω improves prediction of core top Mg/Ca (Brown & Elderfield, 1996; Dekens et al., 2002; Regenberg et al., 2014; Rosenthal et al., 2000; Rosenthal & Boyle, 1993; Russell et al., 1994). Ω sensitivity remains fairly constant across species groups, in agreement with previous work that most species of planktic foraminifera are sensitive to saturation state at the site of deposition (Regenberg et al., 2014). The possible exception is the *N. pachyderma* group, for

Table 2
Regression Model Metrics and Coefficients

	SST	+ Ω^{-2}	+ clean	+ SSS	-SSS + pH
Pooled annual, $n = 710$					
r^2	0.83	0.86	0.87	0.87	0.87
RMSE	0.24	0.22	0.21	0.21	0.21
BIC	2	-135	-198	-210	-193
Coefficient	0.063	-0.35	0.16	0.029	0.30
Pooled seasonal, $n = 710$					
r^2	0.85	0.87	0.89	0.89	0.89
RMSE	0.22	0.21	0.19	0.19	0.19
BIC	-114	-210	-293	-288	-289
Coefficient	0.064	-0.27	0.17	-0.004	0.36
<i>G. ruber</i> , $n = 307$					
r^2	0.55	0.66	0.71	0.71	0.71
RMSE	0.15	0.13	0.12	0.12	0.12
BIC	-284	-363	-407	-403	-404
Coefficient	0.068	-0.24	0.11	0.002	0.28
<i>T. sacculifer</i> , $n = 184$					
r^2	0.51	0.68	0.73	0.73	0.77
RMSE	0.13	0.11	0.10	0.10	0.09
BIC	-214	-287	-318	-314	-339
Coefficient	0.055	-0.27	0.12	0.006	1.4
<i>G. bulloides</i> , $n = 100$					
r^2	0.86	0.88	0.88	0.89	0.89
RMSE	0.19	0.17	0.17	0.17	0.17
BIC	-44	-60	-57	-54	-55
Coefficient	0.068	-0.29	0.12	-0.024	-1.0
<i>N. pachyderma</i> , $n = 119$					
r^2	0.78	0.79	0.80	0.80	0.80
RMSE	0.15	0.15	0.15	0.15	0.15
BIC	-109	-107	-108	-106	-106
Coefficient	0.052	-0.06	0.088	0.047	0.57

Note. Each column notes the addition (or subtraction) of a predictor relative to the column to the left. Group-specific models were calculated with seasonal temperature and salinity estimates. Lower values indicate improved performance. n denotes the number of core tops (after gridding, see section 2). Coefficients correspond to that of the added predictor. Coefficients in italics are not significantly different than zero (at $p = 0.05$). BIC = Bayesian information criterion; RMSE = root mean square error (in $\ln(\text{Mg}/\text{Ca})$ units).

which Ω is not a significant predictor (Table 2). Ω ranges between 0.75 and 2.8 within this group; hence, the lack of sensitivity does not reflect a limitation of the data. It may be that *N. pachyderma* and *N. incompta*, which have a thicker outer calcite crust than the other species considered here, are indeed less sensitive to dissolution, in agreement with buoy exposure experiments (Berger, 1970), although the error on the Ω coefficient is large ($\pm 0.1, 2\sigma$).

3.3. Cleaning

The addition of the cleaning parameter (0 for samples without the reductive step, 1 for samples with the reductive step) improves the statistics for the pooled models and the warm-water groups, with drops in BIC on the order of 10–50 (Table 2) but has little impact on *G. bulloides* and *N. pachyderma*. In the case of *G. bulloides*, this reflects a limitation of the data subset: All but two of the core tops were cleaned with the oxidative protocol, so it is not possible to reliably detect the influence of reductive cleaning. For

N. pachyderma, the influence of cleaning on model skill is small, but the derived coefficient (9%) is close to the other species (11–12%) and is in agreement with previous estimates (Barker et al., 2003; Khider et al., 2015; Rosenthal et al., 2004). Overall, the change in BIC suggests that inclusion of laboratory cleaning does notably improve prediction of core top Mg/Ca and, the limitation of the *G. bulloides* data subset aside, the sensitivity should be relatively consistent across species, as expected from laboratory investigations (Barker et al., 2003).

3.4. Salinity

The addition of salinity to the model does not significantly improve the statistics for the species group regressions, nor for the pooled seasonal model (BIC is mostly unchanged; Table 2). The inferred sensitivity to salinity is low or statistically insignificant in all of these cases. There is moderate improvement in the pooled annual model (BIC drops by 12), and the inferred sensitivity is higher (2.9% per psu), consistent with the best estimate from culture studies ($3.6 \pm 1.2\%$, 2σ ; Gray & Evans, 2019). Overall, these results suggest that the addition of salinity neither improves nor degrades core top Mg/Ca prediction, and furthermore that the derived salinity sensitivity from the core top data set is essentially negligible. This result is not due to our choice to calibrate to surface salinity; derived sensitivities from 0 to 50 m average values yield equally low values (not shown). Rather, the accuracy of the derived salinity sensitivities is restricted by both the limited range of values in our core top data set (95% CI = 33.3 to 37.5 psu) and the strong covariation between temperature and salinity that is typical of global ocean. Since the high latitudes are fresh and cold, and the subtropics warm and salty, below SSTs of 21 ° C, SST and SSS are positively correlated in our data set ($\rho = 0.87$, $p < 0.0001$). Since the tropics are warm and fresh, above 21 ° C SST and SSS are negatively correlated ($\rho = -0.73$, $p < 0.0001$). Even though the direction of the correlation flips, this high degree of relation creates a condition of collinearity, especially for the group data subsets as they fall on one side of the relationship or the other. This means that the OLS-derived coefficients for SSS are not reliable.

3.5. pH

The addition of pH degrades model performance and/or yields insignificant or unrealistic coefficients (Table 2). The expected sensitivity from laboratory experiments is $-70 \pm 14\%$ per pH unit; in comparison, our coefficients are generally of the incorrect sign (Table 2). This is unsurprising given the restricted range of values (8.02–8.17, 95% CI) in our data set and, more broadly, in the modern ocean. In addition, pH is collinear with temperature ($r = -0.70$, $p < 0.0001$), because cold locations have a higher pH. It is also possible that the water column pH observations derived from the GLODAPv2 product are inaccurate. Point GLODAP measurements from the upper water column may not fully sample seasonal and year-to-year variability and include the impact of anthropogenic CO₂, which, in most locations, would not be represented in core top Mg/Ca values. Overall, our regression analysis demonstrates that Mg/Ca sensitivity to pH cannot be reliably recovered from core top data.

3.6. Summary of Environmental Sensitivities

Our iterative regression analysis identifies temperature, Ω , and the laboratory cleaning method as significant predictors of core top Mg/Ca. Salinity and pH sensitivities cannot be accurately determined from the core top data set due to collinearity, a limited range of values, and possible inaccuracies in observations. From an empirical point of view, these findings support the omission of salinity and pH from the Mg/Ca model. However, it is well known from culture studies that salinity and pH are important influences on Mg/Ca and can bias estimates of past temperatures (Gray & Evans, 2019; Khider et al., 2015). We therefore retain these predictors, but in order to provide better constraints on their coefficients, we develop Bayesian hierarchical models in which both the culture and core top data are used to constrain parameters. This model structure leverages the information in both the experimental (laboratory) data and the empirical (core top) data, ultimately allowing for more accurate prediction of Mg/Ca.

4. BAYMAG: Bayesian Calibration Models for Mg/Ca

4.1. Model Design

Following our previous work with $\delta^{18}\text{O}$ of foraminifera (Malevich et al., 2019), we developed two styles of forward models to represent core top Mg/Ca: one that pools all species together (mainly for deep-time applications with extinct species) and another that treats each species group separately, with information

shared through parameters and hyperparameters. The pooled model design is

$$\ln(\mathbf{Mg}/\mathbf{Ca}_c) = \begin{cases} \alpha_i + \mathbf{T}_c \cdot \beta_{Tc} + \mathbf{S}_c \cdot \beta_S + \epsilon_c & \text{if } \textit{incompta}, \textit{sacculifer} \\ \alpha_i + \mathbf{T}_c \cdot \beta_{Tc} + \mathbf{S}_c \cdot \beta_S + \mathbf{pH}_c \cdot \beta_P + \epsilon_c & \text{if } \textit{ruber}, \textit{bulloides}, \textit{universa} \end{cases} \quad (2)$$

$$\epsilon_c \sim \mathcal{N}(\mathbf{0}, \sigma_{\alpha_i}^2),$$

$$\ln(\mathbf{Mg}/\mathbf{Ca}) = \alpha + \mathbf{T} \cdot \beta_T + \mathbf{S} \cdot \beta_S + \mathbf{pH} \cdot \beta_P + \Omega^{-2} \cdot \beta_O + (1 - \mathbf{clean} \cdot \beta_C) + \epsilon, \quad (3)$$

$$\epsilon \sim \mathcal{N}(\mathbf{0}, \sigma^2)$$

with different values of α and σ for each i cultured species. Hyperparameters on the culture temperature coefficient are

$$\beta_{Tc} \sim \mathcal{N}(\mu_{\beta_T}, \sigma_{\beta_T}^2), \quad (4)$$

and the culture temperature coefficient acts as a prior on the core top temperature coefficient:

$$\beta_T \sim \mathcal{N}(\beta_{Tc}, \sigma_{\beta_T}^2). \quad (5)$$

The top of the model hierarchy (equation (2)) describes Mg/Ca in the culture data set (see section 2 for a description of the data compilation) and accounts for the fact that Mg/Ca in cultures of *N. incompta* and *T. sacculifer* is not sensitive to pH (Allen et al., 2016; Davis et al., 2017). Otherwise, the temperature, salinity, and pH sensitivities are assumed to be similar across cultured species, while the intercept and error terms are allowed to vary between each species i to account for offsets in the mean and variance of $\ln(\mathbf{Mg}/\mathbf{Ca})$. As a reality check, we run this top part of the model independently to assess how well it predicts culture Mg/Ca data alone. We find that this top hierarchy yields excellent prediction and the posterior coefficients for temperature, salinity, and pH are similar to previous assessments done with an ordinary least squares approach (Gray & Evans, 2019) (Figure 3), validating our model design.

The lower part of the hierarchy (equation (3)) contains the model for the core top data. Since the core tops are pooled together across all species, it assumes a generic pH sensitivity. The pH and salinity sensitivities (β_P and β_S) are constrained by the culture data in the top part of the hierarchy and then allowed to influence the core top data. Conversely, the sensitivities to Ω and the cleaning method (β_O and β_C) are only constrained by the core top data. The temperature sensitivities β_{Tc} and β_T are constrained by both the culture and core top data, with the former acting as the prior mean for the latter.

The group-specific core top model takes the slightly modified form,

$$\ln(\mathbf{Mg}/\mathbf{Ca}_c) = \begin{cases} \alpha_i + \mathbf{T}_c \cdot \beta_{Tc} + \mathbf{S}_c \cdot \beta_S + \epsilon_c & \text{if } \textit{incompta}, \textit{sacculifer} \\ \alpha_i + \mathbf{T}_c \cdot \beta_{Tc} + \mathbf{S}_c \cdot \beta_S + \mathbf{pH}_c \cdot \beta_P + \epsilon_c & \text{if } \textit{ruber}, \textit{bulloides}, \textit{universa} \end{cases} \quad (6)$$

$$\epsilon_c \sim \mathcal{N}(\mathbf{0}, \sigma_{\alpha_i}^2),$$

$$\ln(\mathbf{Mg}/\mathbf{Ca}) = \begin{cases} \alpha_j + \mathbf{T} \cdot \beta_T + \mathbf{S} \cdot \beta_S + \Omega^{-2} \cdot \beta_O + (1 - \mathbf{clean} \cdot \beta_C) + \epsilon & \text{if } \textit{pachy}, \textit{sacculifer} \\ \alpha_j + \mathbf{T} \cdot \beta_T + \mathbf{S} \cdot \beta_S + \mathbf{pH} \cdot \beta_P + \Omega^{-2} \cdot \beta_O + (1 - \mathbf{clean} \cdot \beta_C) + \epsilon & \text{if } \textit{ruber}, \textit{bulloides} \end{cases}$$

$$\epsilon \sim \mathcal{N}(\mathbf{0}, \sigma_j^2) \quad (7)$$

with hyperparameters and priors on the temperature coefficients as above (equations (4) and (5)). The top part of the hierarchy (equation (6)), describing the culture data, is identical to the pooled model (equation (2)). The lower part of the hierarchy (equation (7)) describes the core top data and, since species are treated independently, accounts for the fact that the *T. sacculifer* and *N. pachyderma* core tops should not be sensitive to pH. As with the culture data, the intercept and error terms (α_j and σ_j) are allowed to vary for each j foraminiferal species. The temperature, salinity, Ω , and cleaning sensitivities are computed across all of the data and are not allowed to vary by species. This choice was made because our regression experiments indicated that, with few exceptions, these sensitivities are similar across species (Table 2). Although we did observe a lower Ω sensitivity for the *N. pachyderma* group (see section 3.2), computation of a hierarchical model with group-specific Ω coefficients yielded no improvement in model skill. Likewise, computation of

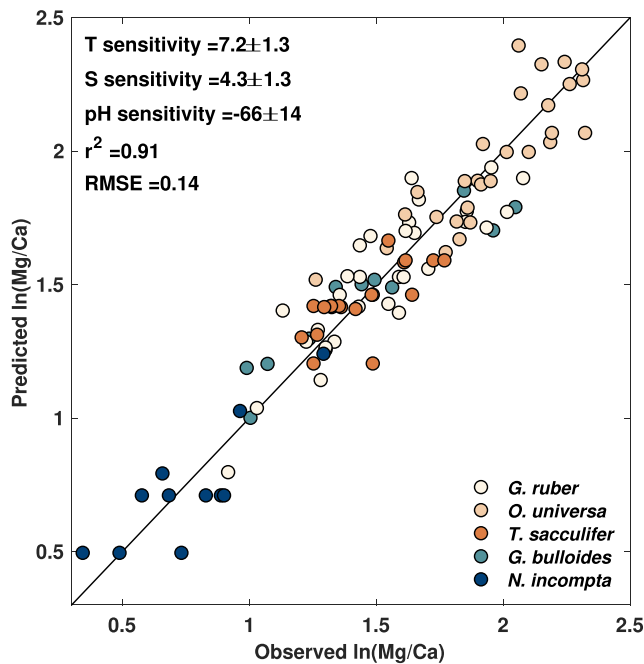


Figure 3. Bayesian hierarchical model results for planktic Mg/Ca culture data, including median and 2σ ranges for the posterior temperature, salinity, and pH sensitivities.

group-specific temperature coefficients did not improve skill, supporting our assumption (and inferences from the culture data) that temperature sensitivity should be similar across species.

For all models, we estimate parameters using Bayesian inference and Markov chain Monte Carlo sampling (Gelman et al., 2003) with Stan software, version 2.19.1 (Carpenter et al., 2017). Prior distributions for the parameters and hyperparameters, as well as prior versus posterior plots, are given in Appendix A. To assess the impact of using annual versus seasonal SST and SSS, we computed the pooled and group-specific models with both sets of values, although we recommend use of either the pooled annual or group-specific seasonal models for practical applications. We perform Pareto-smoothed importance sampling leave-one-out cross-validation to compare predictive accuracy between models (Vehtari et al., 2017). These values are reported as expected log pointwise predictive density (elpd); larger values indicate a better fit to the data.

4.2. Model Results

The pooled annual model explains 87% of the variance in the core top Mg/Ca data and has a median RMSE of 0.21 ln(Mg/Ca) units (Figure 4a). Analysis of the Mg/Ca residuals yields no significant trends with the SST, SSS, Ω , and cleaning predictors. There is a weak correlation between the residuals and core top pH (Spearman's $\rho = 0.15, p < 0.0001$), but as discussed above, we are unsure whether the core top pH observations are accurate. Likewise, the posterior coefficients for the pH predictor are very similar to the those derived from the culture data alone (Figure 3)

reflecting limited influence from the core top data. The derived salinity sensitivity is also close to culture expectations at 3.8%. The median temperature coefficient is lower than the culture value (6.4 vs. 7.2) although by design, is still the same within uncertainty. This shift reflects the influence of the core top data, which act to narrow the temperature sensitivity down to a precise estimate of 6.4 ± 0.2 (2σ).

While as a whole the residuals are well distributed across the zero line, there are systematic offsets according to species (Figure 4b). This is expected, as neither seasonality nor species differences are accounted for in the pooled model. Generally speaking, the model overpredicts Mg/Ca for *N. pachyderma* and *T. sacculifer* (Figures 4d and 4f) and underpredicts Mg/Ca for *G. ruber* and *G. bulloides* (Figures 4c and 4e). These species-level offsets likely reflect differences in depth habitat. *N. pachyderma* is typically interpreted to inhabit the upper 100 m of the water column (Elderfield & Ganssen, 2000; Mortyn & Charles, 2003; Reynolds & Thunell, 1986; Taylor et al., 2018), which would integrate cooler temperatures than SST and lead to lower observed ln(Mg/Ca). This may explain model overestimation in the high latitudes (Figure 4f). Likewise, in the tropics *T. sacculifer* is often found in a slightly deeper habitat than *G. ruber* (Erez & Honjo, 1981; Fairbanks et al., 1980; Ravelo & Fairbanks, 1992), leading to lower Mg/Ca than predicted from surface temperatures. This expected offset between *G. ruber* and *T. sacculifer* can be seen visually in Figure 4a; at higher values of ln(Mg/Ca), *T. sacculifer* plots to the left of *G. ruber*. This explains model overestimation in the tropics (Figure 4d). The pooled model underestimates *G. bulloides* Mg/Ca nearly everywhere, because this species tends to have higher average Mg/Ca values than *N. pachyderma*, *G. ruber*, and *T. sacculifer* (Cléroux et al., 2008; Elderfield & Ganssen, 2000) (Figure 4e).

It is not surprising then that model performance improves markedly with the use of seasonal SST and SSS and group-specific parameters. The most significant improvement comes from accounting for differences between foraminiferal groups (equation (7)), which cause elpd, a measure of predictive accuracy, to rise from 100–150 to 400–450, indicating a much improved fit (Figure 5). The seasonal, group-specific model can account for 95% of the variance in the core top data (Figure 6) with an RMSE comparable to that of the culture regression (Figure 3). As with the pooled model, there is no significant correlation between the cleaning and Ω predictors and the residuals and a weak positive correlation with the pH predictor ($\rho = 0.11, p = 0.003$). There are however weak correlations between the residuals and both temperature and salinity ($\rho = 0.13, p = 0.0008; \rho = -0.21, p < 0.0001$). The negative correlation with salinity is seen in all species groups except *T. sacculifer* and represents the model balance between the strong salinity sensitivity inferred from the

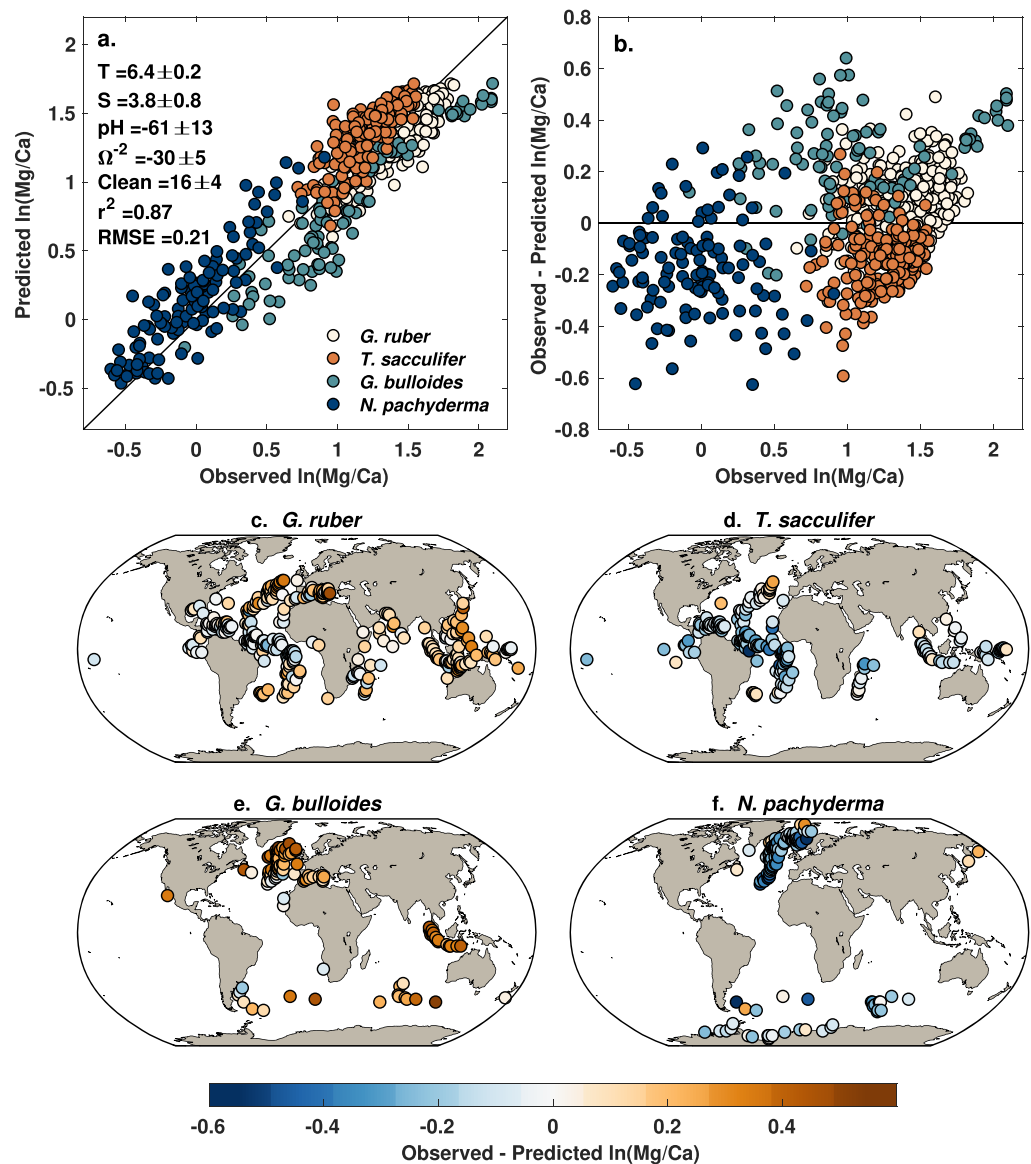


Figure 4. Pooled annual model results. (a) Observed versus predicted $\ln(\text{Mg}/\text{Ca})$, including posterior coefficients for each environmental predictor, colored by species group. (b) Model residuals, colored by species group. (c–f) Maps of model residuals for each species group.

culture data (4.3%, Figure 3) and the weak salinity sensitivity that is recovered from the core top data when seasonal SSTs are used (Table 2). As discussed in section 3.4, the core top-derived salinity sensitivities are affected by collinearity between SST and SSS and therefore may not be accurate. To enforce a sensitivity that is consistent with the culture data, we applied an informative prior to the salinity parameter (see Appendix A). The posterior salinity coefficient is still significantly smaller than that of the pooled model (1.7 ± 0.7 vs. 3.8 ± 0.8) due to core top influence but is higher than it otherwise would be without this constraint.

The correlation between residuals and temperature seems to be mostly driven by *G. ruber* residuals, which also show a strong trend with observed $\ln(\text{Mg}/\text{Ca})$ ($r = 0.70, p < 0.0001$). This could indicate that temperature sensitivity for *G. ruber* is systematically underestimated; however, the trend is only slightly ameliorated after running a version of the group-specific model with variable SST coefficients for each species ($r = 0.61, p < 0.0001$), and the derived ca. 6% sensitivity of the seasonal group-specific model is very similar to values calculated from *G. ruber* culture and sediment trap data (Gray & Evans, 2019; Gray et al., 2018). Alternatively, this residual trend could suggest that our relatively simple inference of seasonal SST

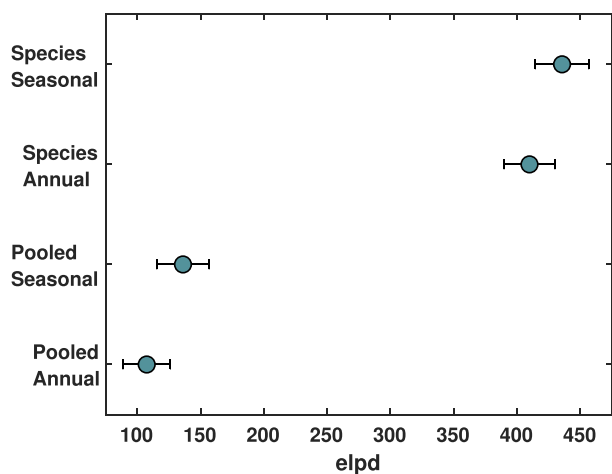


Figure 5. Expected log pointwise predictive density (elpd), based on Pareto-smoothed importance sampling leave-one-out cross-validation, for each Bayesian model. Higher values indicate better fit.

(based on sediment trap abundances) does not apply well to *G. ruber*. However, we did not see this residual trend in our model for $\delta^{18}\text{O}$ of *G. ruber*, which uses the same seasonal estimation method (Malevich et al., 2019). Accounting for subtle differences in depth habitat would make the trend worse, as studies suggest that *G. ruber* should have a deeper habitat in the tropics (and therefore lower Mg/Ca) and shallower one in the subtropics (and therefore higher Mg/Ca) (Hertzberg & Schmidt, 2013; Hönisch et al., 2013). Similar to *G. ruber*, a group of *G. bulloides* data with very high Mg/Ca also falls to the right of the one-to-one line (Figure 6). These data are from the Sumatran margin, where *G. bulloides* calcifies primarily during the cooler upwelling season, at a depth of ca. 50 m (Mohtadi et al., 2009). This preference should cause negative, rather than the observed positive, residuals. Taken together, the *G. bulloides* and *G. ruber* residuals suggest that Mg/Ca sensitivity to temperature may, in fact, be more nonlinear than our model (and all previous exponential models) have assumed or alternatively that there is a latent environmental variable or vital effect that scales nonlinearly with temperature. This latent effect is most prominent in *G. ruber* and accounts for the fact that our model can only explain 67% of the variance in *G. ruber* Mg/Ca. In contrast, our model can explain 73%, 88%, and 77% of the variance in Mg/Ca for *T. sacculifer*, *G. bulloides*, and *N. pachyderma*, respectively.

Further investigation is needed to properly diagnose what this latent variable might be, but the fact that impacts *G. ruber* and *G. bulloides* preferentially suggests that it could be pH. pH scales inversely with temperature; warm locations have lower pH and would be associated with higher Mg/Ca than expected from temperature alone. Although pH is included in our model, if the GLODAP measurements are inaccurate, then this effect would not be fully accounted for in our Mg/Ca predictions and produce the kind of residual trends we observe. Indeed, tropical regions, such as the eastern equatorial Pacific and Indo-Pacific warm pool, are poorly observed in the GLODAP data set, and these are also locations where the residual error is notably low and high, respectively, for *G. ruber* (Figure 6c).

In spite of the residual trends, the magnitude of the residual bias is still very small (0.13 $\ln(\text{Mg/Ca})$ units, 1σ), and out-of-sample applications of BAYMAG in section 5 suggest that our model yields good prediction of *G. ruber* Mg/Ca.

The seasonal group-specific model eliminates the species-level offsets seen in the pooled annual model by allowing the intercept terms to vary for each foraminiferal group (Figure 6b). These intercept terms effectively compensate for depth habitat preference as well as any offsets in average Mg/Ca incorporation. Many of the strong spatial trends in residuals are also minimized (Figures 6c–6f) when compared to the pooled model (Figures 4c–4f), although some patterns remain. In addition to patterns that may reflect the impact of the latent variable discussed above, there are negative residuals for *G. bulloides* in the west African and Benguela upwelling zones; along frontal regions in the Southern Ocean; and near the confluence of the Brazil and Malvinas currents (Figure 6e) indicating that Mg/Ca values are lower than the model predicts. Similar patterns were observed in the residuals of our Bayesian $\delta^{18}\text{O}$ models (Malevich et al., 2019) and might suggest that *G. bulloides* is calcifying during either a cooler season than our seasonal SST inferences predict or in a deeper habitat. These patterns could also conceivably reflect geochemical differences between *G. bulloides* genotypes (Sadekov et al., 2016) or high productivity driving locally enhanced dissolution (Hertzberg & Schmidt, 2013).

5. Application of the BAYMAG Forward Model

Forward modeling of Mg/Ca is useful for model-data comparison and data assimilation techniques that rely on forward models to translate model output into proxy units (Hakim et al., 2016). BAYMAG can be used to model new values of Mg/Ca (\tilde{y}) from observed or simulated SST, SSS, pH, Ω , and cleaning protocol by simply drawing from the posterior predictive distribution, $\tilde{y} \sim \mathcal{N}(\mu, \sigma^2)$, where μ and σ are the core top component

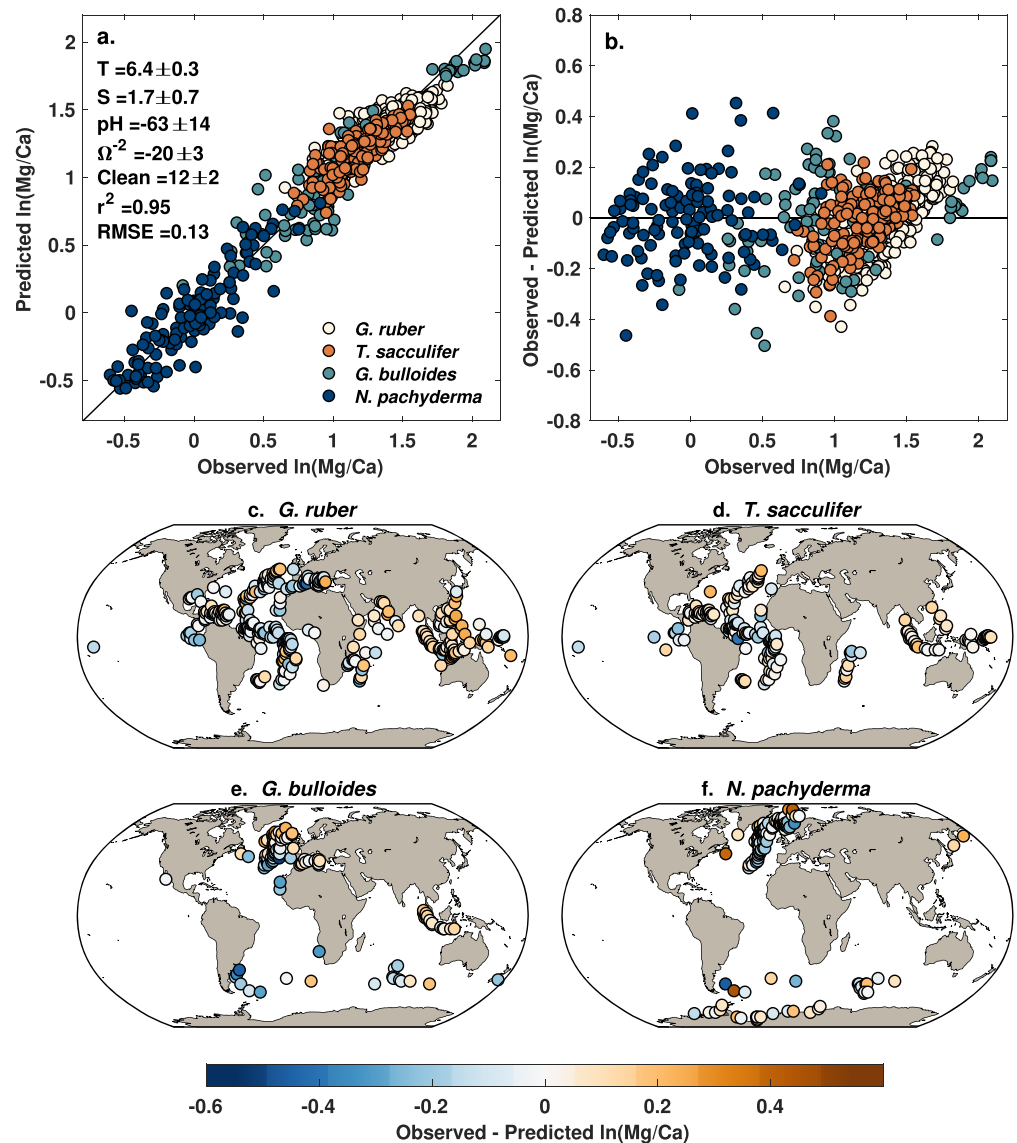


Figure 6. Seasonal, group-specific model results. (a) Observed versus predicted ln(Mg/Ca), including posterior coefficients for each environmental predictor, colored by species group. (b) Model residuals, colored by species group. (c–f) Maps of model residuals for each species group.

of either the pooled annual or group-specific seasonal model (equations (3) and (7)). If the user desires, a prior can be used to restrict values to reasonable outcomes; for example, for *G. ruber*, Mg/Ca values over 6.5 are rarely observed in the modern ocean (0% of core tops and 1% of sediment traps). To provide an example, as well as to test our model on out-of-sample data, we apply BAYMAG to monthly average observations of SST, SSS, and pH at two locations that have multi-year foraminiferal Mg/Ca sediment trap data (Figure 7). For the Gulf of Mexico site, we used the SST, SSS, and pH climatologies (adjusted values) provided in the source publication (Richey et al., 2019). For the Gulf of California site, we used average monthly SSTs reported in the source publication (McConnell & Thunell, 2005), WOA13 climatology for SSS, and pH climatology as estimated by Gray et al. (2018). Ω is set to 5.7 for the Gulf of Mexico and 3.4 for the Gulf of California; since these values are high, they have minimal impact on predicted Mg/Ca. Both studies used a nonreductive cleaning protocol, so the cleaning value is set to 0. In all cases we use the group-specific, seasonal model; although temperatures and salinity vary month by month in this case, we assume that the seasonal model most accurately captures the “true” environmental sensitivities. Weak priors on Mg/Ca were used to assign a low probability (< 5%) to Mg/Ca values above 7 and 9 for *G. ruber* and *G. bulloides*, respectively (Figure 7).

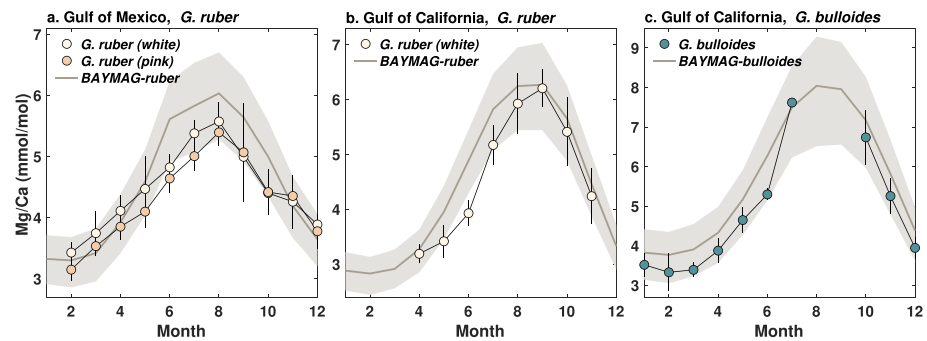


Figure 7. Forward-modeled Mg/Ca from BAYMAG, compared to sediment trap observations from the Gulf of Mexico (Richey et al., 2019) and Gulf of California (McConnell & Thunell, 2005). Normal priors of $\mathcal{N} \sim (4, 1.5)$ and $\mathcal{N} \sim (5, 2)$ were used for *G. ruber* and *G. bulloides*, respectively. The Gulf of Mexico data were shifted backwards by 1 month to account for sinking and integration time. No adjustments to the Gulf of California data were made; this is a shallower trap (485 vs. 1,150 m), and the data indicate minimal lag. Shading and error bars represent 1σ uncertainties.

Overall, the BAYMAG predictions match observed Mg/Ca values well, almost always overlapping within the 1σ range (Figure 7). This is an encouraging result, because our model is calibrated on core top foraminifera that have been affected by dissolution and sedimentary processes, while the sediment trap data consist of more pristine specimens. BAYMAG slightly overestimates *G. ruber* Mg/Ca in the Gulf of Mexico (Figure 7a), even though our model residuals suggest that it should underpredict high values (Figure 6b), suggesting that the residual trends have a minimal impact on prediction.

6. Inversion of BAYMAG to Predict Past SST

Since BAYMAG is a multivariate model, inversion to predict past SSTs requires constraints on salinity, pH, and Ω . In the simplest case, these can be held constant at modern values, but this assumes that only temperature caused observed variation in Mg/Ca. More realistic inference can be derived from making informed assumptions about past changes. For example, over the Quaternary glacial cycles, it is reasonable to assume that surface water pH and salinity both increased during glacial periods due to lower atmospheric CO_2 and lower sea level. It is also possible to leverage information from independent proxies sensitive to changes in the oceanic carbonate system, such as $\delta^{11}\text{B}$ (for surface pH) or benthic B/Ca (for Ω). Alternatively, output from a climate or biogeochemical model could be used to provide constraints.

To facilitate SST prediction for diverse applications, we provide two versions of the Bayesian inverse model for Mg/Ca. One assumes that salinity, pH, and Ω are known, allowing for quick computation of posterior SST. The other treats all of the environmental predictors as unknowns and allows the user to place prior distributions on them. This latter model involves joint computation of posterior temperature, salinity, pH, and Ω and is therefore slower to converge but has the advantage of propagating uncertainty in these covariates into the estimation of SST.

To demonstrate use of the inverse models, we apply BAYMAG to three sites that have Late Quaternary Mg/Ca data as well as independent estimates of SST from alkenone $U_{37}^{K'}$ (Figure 8a). In each case, we use the appropriate seasonal, group-specific model; however, our KDE method for inferring seasonality predicts that foraminifera at all three of these locations should reflect mean annual temperature. We draw modern Ω and surface pH value for each site from GLODAPv2 (Lauvset et al., 2016) and modern salinity from WOA13 (Boyer et al., 2013). In all cases, we use a prior standard deviation of 6°C and assume that pH, salinity, and Ω are error free; we found that including errors on these factors only slightly increases error bars (not shown).

For the Holocene data at site MD99-2269 in the North Atlantic, we assume that salinity, and Ω are constant through time (*N. pachyderma* is not sensitive to pH). We find that BAYMAG predicts latest Holocene SST values that are in good agreement with modern observed annual SST, whereas the calibration (Elderfield & Ganssen, 2000) used in the original publication (Kristjánsson et al., 2017) slightly underestimates SSTs (Figure 8b). The BAYMAG predictions suggest that annual SSTs have declined through the Holocene by about 3°C . In contrast, the $U_{37}^{K'}$ data from this site show a weaker long-term trend and are also much warmer

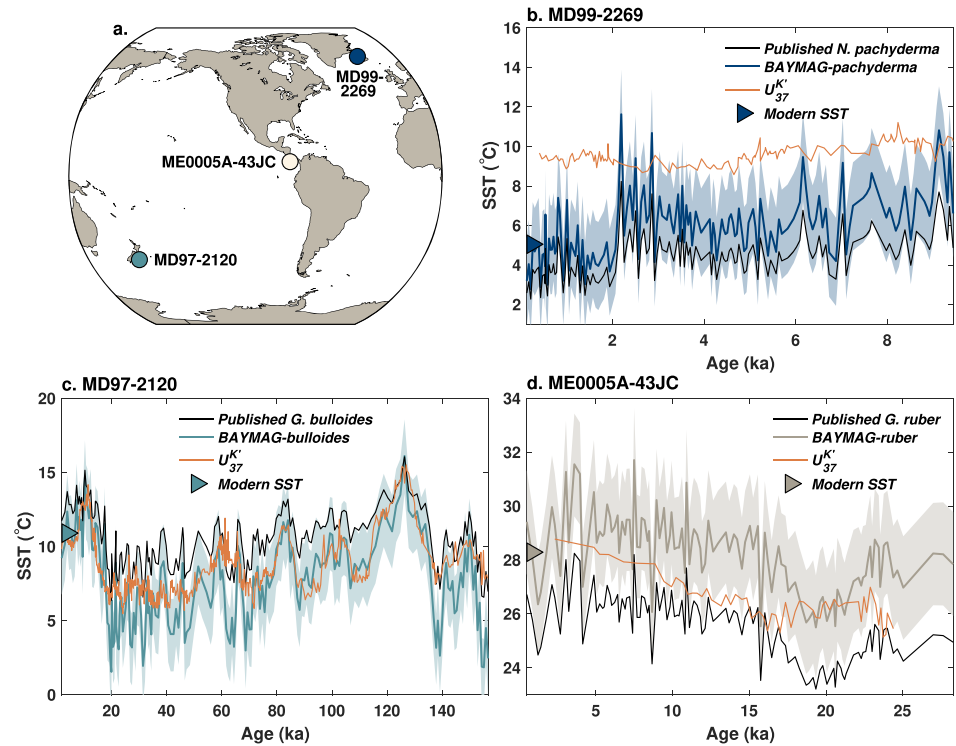


Figure 8. Example applications of BAYMAG to predict past SSTs. (a) Locations of targeted Late Quaternary sites. (b) *N. pachyderma* data from MD99-2269 (66.6°N, 20.9°W, 365 m, Kristjánsdóttir et al., 2017). (c) *G. bulloides* data from MD97-2120 (45.5°S, 174.9°E, 1210 m, Pahnke et al., 2003). (d) *G. ruber* data from ME0005A-43JC (7.9°N, 83.6°W, 1368 m, Benway et al., 2006). At each location, data are compared to $U_{37}^{K'}_{37}$ SST estimates (median values, calibrated with BAYSPLINE, Tierney & Tingley, 2018). Triangles show modern mean annual SSTs at each site. Shading indicates 1σ uncertainties.

than the *N. pachyderma* predictions (Figure 8b). $U_{37}^{K'}_{37}$ at this latitude (66° N) is assumed to reflect late summer temperatures (August–October) (Tierney & Tingley, 2018); however, modern August–October SSTs at this site (6.4 °C) are still much cooler than the latest Holocene $U_{37}^{K'}_{37}$ values (ca. 9.5 °C, Figure 8b). This might indicate that $U_{37}^{K'}_{37}$ production is restricted to only the warmest of summer months; alternatively, the warm bias could reflect the influence of sea ice. This site sits close to the boundary where substantial seasonal sea ice is present in the modern day, and anomalously high $U_{37}^{K'}_{37}$ values occur in areas of extensive sea ice cover (Filippova et al., 2016; Tierney & Tingley, 2018).

For site MD97-2120 in the South Pacific, we make some rudimentary assumptions of how pH and salinity may have varied over glacial-interglacial cycles. Following Gray et al. (2018) and Gray and Evans (2019), we assume that global pH increased by 0.13 units during the Last Glacial Maximum (LGM) due to lowered CO_2 . We then scaled the normalized ice core CO_2 curve (Bereiter et al., 2015) to this value and added it to the modern site estimate of pH to simulate past changes. For this site, this results in a range of pH values between 8.12 (modern value) and 8.25 (maximum glacial value). For salinity, we scaled the normalized sea level curve to an inferred LGM change of 1.1 psu and added this to the site estimate, for a range between 34.4 (modern values) and 35.5 (maximum glacial value). We then interpolate these scaled curves to the ages at which there are Mg/Ca observations and input them into BAYMAG. We do not explicitly account for the temperature effect on pH (e.g., Gray & Evans, 2019) because while it scales with the magnitude of local cooling, it is a small source of error for the LGM (0.65°C, Gray & Evans, 2019). Since the salinity and pH sensitivities are of opposite sign, the glacial-interglacial changes partly cancel each other out; however, LGM cooling is still 0.8 °C warmer than estimates made with constant salinity and pH (not shown) due to the pH effect.

The BAYMAG predictions from *G. bulloides* Mg/Ca at MD97-2120 produce latest Holocene SSTs in good agreement with modern mean annual values and yield cooler median values and a larger glacial-interglacial

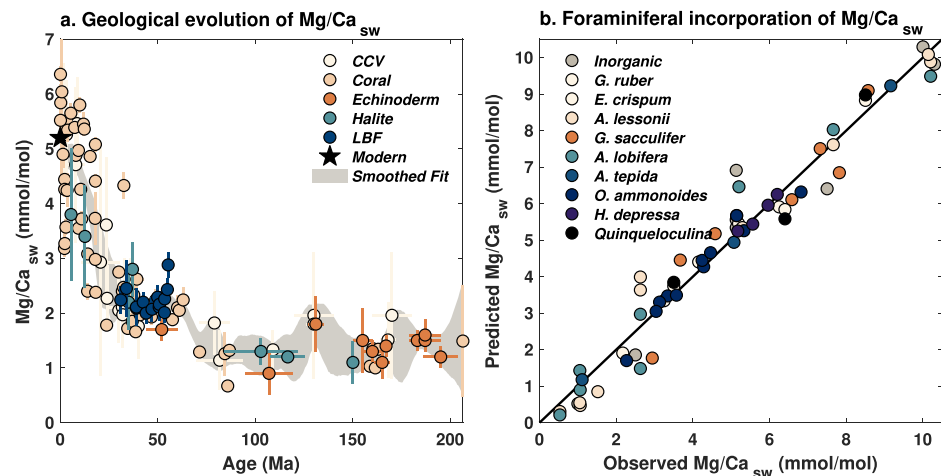


Figure 9. (a) Evolution of $\text{Mg}/\text{Ca}_{\text{sw}}$ over the past 200 Ma, according to Mg/Ca measured in calcium carbonate veins (CCV, Coggon et al., 2010), fossil corals (Gothmann et al., 2015), echinoderm ossicles (Dickson, 2002; Dickson, 2004), halite fluid inclusions (Brennan et al., 2013; Horita et al., 2002; Lowenstein et al., 2001), and large benthic foraminifera (LBF, Evans et al., 2018). Star denotes the modern value of 5.2 mmol/mol (Horita et al., 2002). Shading encloses the 95% CI of an ensemble of Gaussian smoothed fits to the data, used in the seawater-enabled BAYMAG models. (b) Relationship between observed $\text{Mg}/\text{Ca}_{\text{sw}}$ and linear predictions of $\text{Mg}/\text{Ca}_{\text{sw}}$ from Mg/Ca of calcite in laboratory inorganic precipitation (Mucci & Morse, 1983) and foraminiferal culture studies (De Nooijer et al., 2017; Delaney et al., 1985; Evans et al., 2015; Evans, Brierley, et al., 2016; Hauzer et al., 2018; Mewes et al., 2014; Raitzsch et al., 2010; Segev & Erez, 2006).

range than the calibration (Mashiotta et al., 1999) used in the original publication (Pahnke et al., 2003) (Figure 8c). There is generally a good match with alkenone $U_{37}^{K'}$, except during the coldest times of the glacial periods (Figure 8c). The cold predictions in part reflect the fact that the glacial *G. bulloides* Mg/Ca values at this site are at the limit of the modern calibration data set, and the group-specific model has a tendency to overpredict Mg/Ca (and thus underpredict SSTs) at southern latitudes (Figure 6e). A tighter prior could mitigate this effect; however, this example illustrates that caution should be exercised when extrapolating BAYMAG to values of Mg/Ca that are near the edge or outside of the calibration range.

Finally, we tested BAYMAG on *G. ruber* data from site ME0005A-43JC, in the eastern Pacific warm pool. We scale salinity and pH estimates in the same manner as at site MD97-2120. Varying salinity and pH results in glacial estimates that are ca. 0.9°C warmer than a constant assumption (not shown). Latest Holocene BAYMAG predictions once again align well with modern SSTs and are overall warmer than the published estimates (Benway et al., 2006), which used the Anand et al. (2003) calibration without a correction for dissolution (Figure 8d). Although this site is not particularly deep, it sits in a relatively corrosive location—modern Ω is 0.95—thus, BAYMAG assumes some Mg/Ca loss from dissolution. The magnitude of glacial cooling agrees well with the $U_{37}^{K'}$ estimates, although the two proxies have different trajectories through the deglaciation and the Holocene (Figure 8d). The different trajectories could reflect differences in the seasonal production of alkenones and *G. ruber* (Timmermann et al., 2014); however, core top studies in the eastern equatorial Pacific do not find any evidence for a seasonal bias in alkenone signatures (Kienast et al., 2012; Tierney & Tingley, 2018).

7. Use of BAYMAG on Longer Geological Timescales

7.1. Incorporating Changes in Mg/Ca of Seawater

When Mg/Ca is used to infer SSTs on million-year timescales, data must be corrected for secular changes in the Mg/Ca ratio of seawater ($\text{Mg}/\text{Ca}_{\text{sw}}$). Ancient $\text{Mg}/\text{Ca}_{\text{sw}}$ values can be independently estimated from fossil corals (Gothmann et al., 2015), halite fluid inclusions (Brennan et al., 2013; Horita et al., 2002; Lowenstein et al., 2001), calcium carbonate veins (Coggon et al., 2010), echinoderm ossicles (Dickson, 2002; Dickson, 2004), and paired Mg/Ca -clumped isotope measurements of benthic foraminifera (Evans et al., 2018). Although some of these $\text{Mg}/\text{Ca}_{\text{sw}}$ estimates have large uncertainties and are also sometimes poorly dated,

they clearly indicate a nonlinear increase in $\text{Mg}/\text{Ca}_{\text{sw}}$ over the past 200 Ma, with the most rapid change occurring in the last 30 Ma (Figure 9a). The reason for the increase is still not certain; magnesium isotope evidence and geochemical modeling suggest that it could reflect a decrease in Mg incorporation into marine clays (Dunlea et al., 2017; Higgins & Schrag, 2015).

To develop a version of BAYMAG that accounts for changing $\text{Mg}/\text{Ca}_{\text{sw}}$, we created a 1,000-member ensemble of possible $\text{Mg}/\text{Ca}_{\text{sw}}$ trajectories by Monte Carlo sampling the uncertainties in both age assignment and $\text{Mg}/\text{Ca}_{\text{sw}}$ of each estimate in Figure 9a, interpolating to a 0.5 Ma time step, and applying a 13 Ma (the residence time of Mg) Gaussian smooth (Figure 9a). The resulting collection of curves is then used to calculate $\text{Mg}/\text{Ca}_{\text{sw}}$ for each time t for a given Mg/Ca data series and then used in the prediction model, that is:

$$\ln(\mathbf{Mg}/\mathbf{Ca}) = \alpha_j + \mathbf{T} \cdot \beta_T + \mathbf{S} \cdot \beta_S + \mathbf{pH} \cdot \beta_P + \Omega^{-2} \cdot \beta_O + (1 - \mathbf{clean} \cdot \beta_C) + \frac{\text{Mg}/\text{Ca}_{\text{sw}_t}}{\text{Mg}/\text{Ca}_{\text{sw}_0}} + \epsilon, \quad (8)$$

$$\epsilon \sim \mathcal{N}(\mathbf{0}, \sigma_\epsilon^2).$$

Previous work has suggested that the incorporation of Mg into calcite varies nonlinearly with $\text{Mg}/\text{Ca}_{\text{sw}}$, necessitating a power function correction (Evans & Müller, 2012), rather than a simple ratio between the past value and the modern value as we suggest above. To re-examine whether such an adjustment is necessary, we compiled experimental data in which planktic and benthic foraminifera were cultured at varying $\text{Mg}/\text{Ca}_{\text{sw}}$ concentrations (De Nooijer et al., 2017; Delaney et al., 1985; Evans et al., 2015; Evans, Brierley, et al., 2016; Hauzer et al., 2018; Mewes et al., 2014; Raitzsch et al., 2010; Segev & Erez, 2006), along with an inorganic precipitation experiment (Mucci & Morse, 1983) (Figure 9b). These data span values of $\text{Mg}/\text{Ca}_{\text{sw}}$ from 0.5 to 10 mmol/mol (Figure 9b), which encompasses the range found throughout the Phanerozoic (0.5–6 mmol/mol, Dickson, 2002; Dickson, 2004). For each species (and the inorganic experiment), we computed an ordinary least squares regression between $\text{Mg}/\text{Ca}_{\text{sw}}$ and Mg/Ca_c and used the resulting coefficients to predict $\text{Mg}/\text{Ca}_{\text{sw}}$ from Mg/Ca_c . If there were a nonlinear relationship between $\text{Mg}/\text{Ca}_{\text{sw}}$ and Mg/Ca_c , then the predictions should show curvature away from the 1:1 line. We find that when all the experiments are considered together, this is not the case—a power function fit to the predictions, of the form $y = a \times x^b$, yields a value of b close to 1 (0.97 ± 0.07 , 2σ) suggesting no significant curvilinear behavior. Power fits to predictions from individual species (and the inorganic experiment) also yield values of b insignificantly different from 1, confirming that the relationship between $\text{Mg}/\text{Ca}_{\text{sw}}$ and Mg/Ca_c is adequately described by a linear function. The slope of this relationship varies substantially between species; however, since $\text{Mg}/\text{Ca}_{\text{sw}}$ is ratioed to the modern value (equation (8)), this term cancels out. This analysis does not preclude nonlinear incorporation of Mg into calcite at very low $\text{Mg}/\text{Ca}_{\text{sw}}$ concentrations (<0.5 mmol/mol); however, such concentrations are not observed in the Phanerozoic. Thus, we conclude that a power function adjustment is not necessary for paleoclimate applications.

More recently, it has been proposed that the temperature sensitivity of Mg/Ca in foraminifera changes with $\text{Mg}/\text{Ca}_{\text{sw}}$ (Evans, Brierley, et al., 2016). However, thus far this has only been detected in a culture experiment of *G. ruber*; a study of benthic foraminiferal species did not detect a change in temperature sensitivity with $\text{Mg}/\text{Ca}_{\text{sw}}$ (De Nooijer et al., 2017). We therefore do not incorporate this aspect into our model; further experimental evidence supporting this effect is needed.

7.2. Applications

To test our $\text{Mg}/\text{Ca}_{\text{sw}}$ -enabled models, we apply BAYMAG to representative Cenozoic Mg/Ca data. First, we use the seasonal, group-specific model to predict SSTs from *T. sacculifer* data from Site ODP 806, in the western Pacific warm pool (Wara et al., 2005). We assume that salinity and pH are constant through time and error free and use a prior standard deviation of 6°C (Figure 10a). These data span the early Pliocene (5.3 Ma) to present, over which time $\text{Mg}/\text{Ca}_{\text{sw}}$ has evolved from 4.8 ± 0.2 (2σ) mmol/mol to the current value of 5.2 mmol/mol, according to our ensemble estimate. Although this is a small change, it does impact SST prediction, as can be seen from comparison with the published SST estimates (Wara et al., 2005), which use the Dekens et al. (2002) calibration and did not account for changing $\text{Mg}/\text{Ca}_{\text{sw}}$ (Figure 10a). Whereas the original SST estimates suggest that Pliocene SSTs were consistently cooler than modern, the BAYMAG estimates indicate that they were mostly similar to, or warmer than, modern values and bring the data into better agreement with independent estimates from the TEX_{86} proxy (Zhang et al., 2014) (Figure 10a).

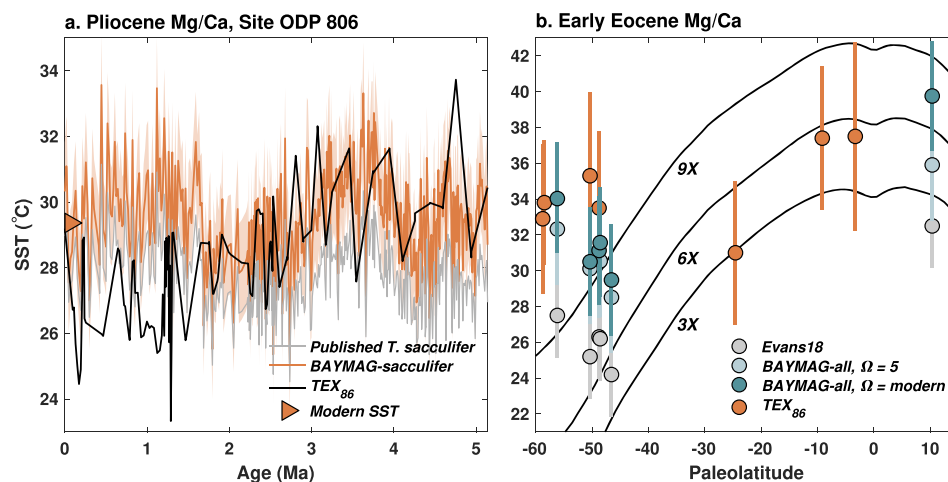


Figure 10. Application of BAYMAG to Cenozoic Mg/Ca data, with correction for changing Mg/Ca_{sw} . (a) Mg/Ca data extending back to the Pliocene from Site ODP 806 (Wara et al., 2005). Triangle indicates modern mean annual SST. (b) Mg/Ca data (Hines et al., 2017; Hollis et al., 2009; Hollis et al., 2012; Tripathi et al., 2003) from the Early Eocene Climatic Optimum (53.3–49.1 Ma), plotted by paleolatitude. Black lines denote predicted SSTs from Eocene climate model simulations conducted under 3 \times , 6 \times , and 9 \times preindustrial CO_2 levels (Zhu et al., 2019). In both panels, TEX_{86} data (calibrated with BAYSPAR, Tierney & Tingley, 2014) are plotted for comparison. Shading and error bars represent 1σ uncertainties.

Next, we apply BAYMAG to Mg/Ca data from the Early Eocene Climatic Optimum (EECO, 53.3–49.1 Ma), one of the warmest times during the Cenozoic Era. These data include *Morozovella* spp. from site ODP 865 (Tripathi et al., 2003), hemipelagic outcrops from the eastern shore of New Zealand (mid-Waipara, Tawanui, Tora, and Hampden Beach, Hollis et al., 2009, 2012; Hines et al., 2017), and DSDP Site 277 (Hines et al., 2017). *Morozovella* spp. species are extinct, so we do not know their seasonal or depth habitat preferences. Thus, we use the pooled annual model, which provides generic constraints on temperature, salinity, pH, and Ω sensitivities. Following Evans et al. (2018), we assume, based on carbon modeling constraints (Tyrrell & Zeebe, 2004), that ocean pH is approximately 7.7 during the EECO. Since we have no good knowledge of how salinity changed, we hold it constant at a value of 34.5 for each site. For Ω , we test two assumptions: (1) that the foraminifera are essentially pristine, unaltered by seafloor dissolution ($\Omega = 5$), and (2) that the foraminifera have experienced dissolution on par with what we would expect at the site locations today. For this latter assumption, we draw Ω from GLODAPv2 using the paleolatitude and paleolongitude (calculated from Baatsen et al., 2016, as suggested in Hollis et al., 2019) and the inferred Eocene water depth as described in the original publication. We use an uninformative prior standard deviation of $10^\circ C$.

We compare our results to the inferences made by Evans et al. (2018) using the same Mg/Ca data, as well as independent estimates of SST from EECO TEX_{86} data spanning similar paleolatitudes (Bijl et al., 2009; Bijl et al., 2013; Cramwinckel et al., 2018; Hollis et al., 2009, 2012; Inglis et al., 2015; Pearson et al., 2007) calibrated with BAYSPAR (Hollis et al., 2019; Tierney & Tingley, 2014) (Figure 10b). All of the estimates from BAYMAG are warmer, on average, than those of Evans et al. (2018), by $4.3^\circ C$ under the assumption of no dissolution, and by $5.8^\circ C$ with modern Ω estimates (Figure 10b). Since our inferred Mg/Ca_{sw} value for the Eocene (2.2 mmol/mol) is the same as Evans et al. (2018), this difference reflects model form. Evans et al. (2018) first correct Mg/Ca for the pH effect using laboratory constraints (Evans, Wade, et al., 2016) and then calculate SST assuming a reduced temperature sensitivity at lower Mg/Ca_{sw} , using coefficients derived from *G. ruber* culture experiments (Evans, Brierley, et al., 2016).

In the absence of information concerning the Eocene carbonate system, Evans et al. (2018) assume no loss from dissolution at depth. For shallow and intermediate-depth sites considered here, allowing some dissolution increases median SST estimates up by 0.3 – $1.5^\circ C$ —a relatively minor effect. ODP 865 is an exception: Here, using a modern estimate of Ω yields median SST estimates that are $3.9^\circ C$ higher. This is because plate rotations (Baatsen et al., 2016; Herold et al., 2014) predict that this site was located much closer to the equator (4 – $10^\circ N$, vs. $18^\circ N$ today) and farther east (138 – $144^\circ W$, vs. $179^\circ W$ today) during the EECO. Today, the

eastern equatorial Pacific is very corrosive, even at intermediate water depths. If EECO Pacific ocean chemistry was similar, then the Mg/Ca values at ODP 865 would imply very high SSTs (ca. 39 ° C, Figure 10b). This illustrates how assumptions about Ω can have a large impact on SST estimation from Mg/Ca measured in pelagic settings, especially over timescales when ocean chemistry may have changed substantially.

BAYMAG SST predictions agree more closely with EECO TEX₈₆ data than the Evans et al. (2018) calculations (Figure 10b). Tropical SSTs inferred from Site 865 support TEX₈₆ inferences of ca. 36 ° C and match output from an Eocene climate model simulation run under 6× preindustrial CO₂ (Zhu et al., 2019). The Mg/Ca predictions support TEX₈₆ in detecting unusually high SSTs at sites near New Zealand (50–55° S paleolatitude) that are not easily explained by elevated CO₂; these data may reflect changes in ocean circulation leading to localized warming (Hollis et al., 2009) (Figure 10b).

8. Conclusions

The Mg/Ca paleothermometer is complex. It is sensitive to multiple environmental factors, which challenges both calibration and application. Traditionally, Mg/Ca applications have “precorrected” the data for factors such as dissolution, laboratory cleaning method, or pH sensitivity (e.g., Evans et al., 2018; Gray & Evans, 2019; Rosenthal & Lohmann, 2002). While effective, this makes uncertainty propagation challenging. A clear advantage of our BAYMAG models is that all known environmental sensitivities are included in a single model framework, making pre-correction obsolete. Furthermore, we show that we can account for most of the variance in the Mg/Ca of core top data through use of a hierarchical Bayesian model structure that leverages both culture and core top constraints on environmental sensitivities. Encouragingly, temperature remains the most important predictor of Mg/Ca, followed by bottom water calcite saturation state (Ω). Salinity and pH sensitivities are essentially undetectable in core top data; hence, culture constraints are key.

The BAYMAG hierarchical models fit the data well, although some species, most notably *G. ruber*, still have trends in their residuals suggesting that some variance is left unexplained. Future work will be needed to identify why this is the case; we hypothesize that there is latent covariate that scales with temperature (possibly pH). Fortunately, the absolute magnitude of the residuals is small, such that the trends typically do not bias predicted values. Indeed, applications of BAYMAG demonstrate that it yields reasonable forward predictions of Mg/Ca when compared to sediment trap observations and reasonable inverse predictions when compared to independent SST proxies. The latter is true even though strong—and potentially incorrect—assumptions about past changes in Ω , salinity, and pH must be made. Deep-time applications must additionally account for changing Mg/Ca_{sw}. We use independent constraints on the evolution of Mg/Ca_{sw} to develop a smoothed ensemble estimate for use with BAYMAG. Example applications once again suggest good agreement with independent SST proxies, but there can be large uncertainties in absolute SST estimates when potential changes in Ω in particular are considered.

In this work, we seek to develop prediction models for Mg/Ca of foraminifera that are independent from other proxy systems. However, given the multivariate nature of Mg/Ca, it would be beneficial to use information from other temperature proxies in a formal hierarchical model structure. Previous work has already explored this avenue by combining Mg/Ca measurements with TEX₈₆ or $\Delta 47$ to estimate Mg/Ca_{sw} (e.g., Evans et al., 2018; Evans, Brierley, et al., 2016; O'Brien et al., 2014) and by combining Mg/Ca with $\delta^{18}\text{O}$ to infer $\delta^{18}\text{O}_{\text{sw}}$ or salinity (e.g., Oppo et al., 2009; Thirumalai et al., 2016; Tierney et al., 2016). Future work might explore incorporating $\delta^{11}\text{B}$ and B/Ca estimates of pH and calcite saturation state, respectively. This would almost certainly improve past estimates of SST, especially over timescales when ocean carbonate chemistry is expected to have changed substantially.

Appendix A: BAYESIAN REGRESSION MODEL PRIORS

Priors for the Bayesian regression parameters were chosen so as to enforce the expected direction of the sensitivity based on geochemistry (e.g., Mg/Ca increases with temperature but decreases with Ω^{-2}) but otherwise be only weakly informative, with the exception of the salinity prior. The salinity sensitivity was explicitly bounded by the posterior value for β_S from culture data ($4.3 \pm 1.3\%$, 2σ) to counteract the tendency of the core tops to dilute the sensitivity. Slightly different priors for the pooled and group-specific models were used for the $\sigma_{\beta_{TC}}$ and σ parameters:

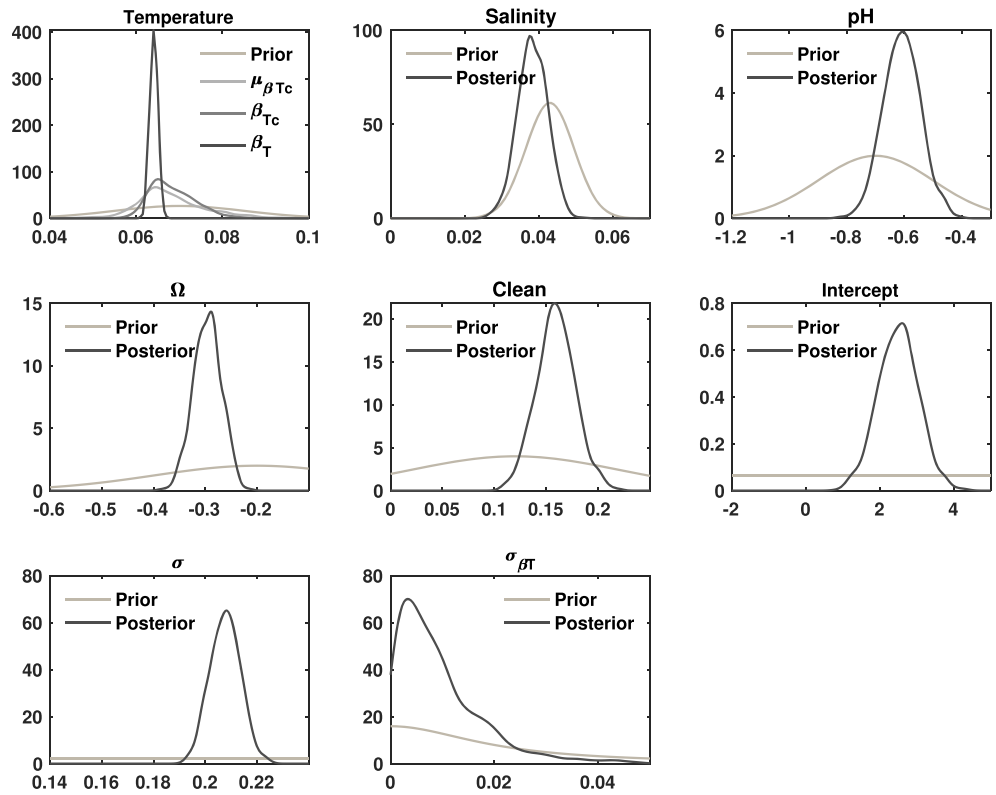


Figure A1. Prior and posterior parameter distributions for the pooled annual model.

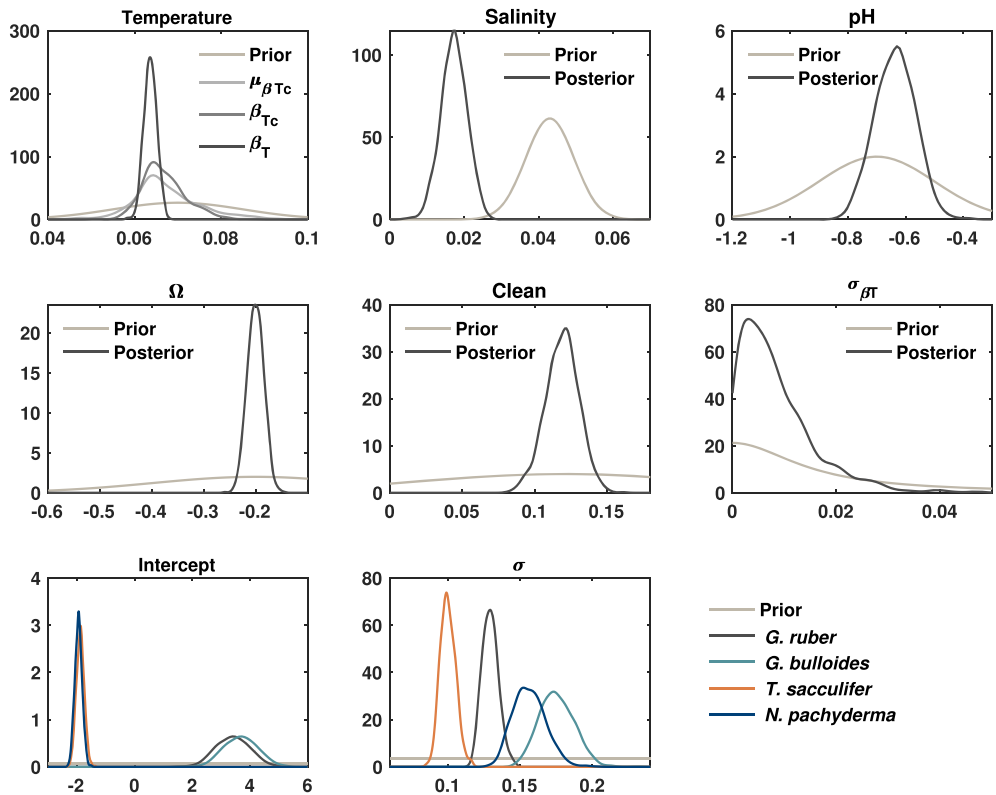


Figure A2. Prior and posterior parameter distributions for the group-specific seasonal model.

$$\begin{aligned}
 \alpha &\sim \mathcal{U}(-5, 10), \\
 \mu_{\beta Tc} &\sim \mathcal{N}_{[0, \infty)}(0.07, 0.015), \\
 \sigma_{\beta Tc} &\sim \text{HalfCauchy}(0.02)_{[\text{pooled}]}; \sim \text{HalfCauchy}(0.015)_{[\text{species}]} \\
 \beta_S &\sim \mathcal{N}_{[0, \infty)}(0.043, 0.0065), \\
 \beta_P &\sim \mathcal{N}_{(\infty, 0]}(-0.7, 0.2), \\
 \beta_O &\sim \mathcal{N}_{(\infty, 0]}(-0.2, 0.2), \\
 \beta_C &\sim \mathcal{N}_{[0, \infty)}(0.12, 0.1), \\
 \sigma &\sim \mathcal{U}(0, 0.5)_{[\text{pooled}]}; \sim \mathcal{U}(0, 0.3)_{[\text{species}]}.
 \end{aligned}
 \tag{A1}$$

Plots of the prior versus posterior distributions for the pooled annual and group-specific seasonal models are shown below. Note that the temperature panel contains posteriors for the hyperparameter $\mu_{\beta Tc}$, the culture data parameter β_{Tc} , and the core top data parameter β_T .

Acknowledgments

This work was supported by National Science Foundation (NSF) Grant AGS-1602301, Heising-Simons Foundation Grant 2016-015, and the Packard Fellowship in Science and Engineering to J. T. We thank Dr. David Evans, Dr. Jennifer Hertzberg, and one anonymous reviewer for valuable comments that improved the manuscript. BAYMAG code (in MATLAB) is available on GitHub (<https://github.com/jesstierney/BAYMAG>). Compiled core top, culture, and Mg/Ca of seawater data are available in the Supporting Information, as well as online in the Pangaea database (<https://doi.pangaea.de/10.1594/PANGAEA.908097>).

References

- Aagaard-Sørensen, S., Husum, K., Hald, M., Marchitto, T., & Godtlielsen, F. (2014). Sub sea surface temperatures in the Polar North Atlantic during the Holocene: Planktic foraminiferal Mg/Ca temperature reconstructions. *The Holocene*, *24*, 93–103. <https://doi.org/10.1177/0959683613515730>
- Allen, K. A., Hönisch, B., Eggins, S. M., Haynes, L. L., Rosenthal, Y., & Yu, J. (2016). Trace element proxies for surface ocean conditions: A synthesis of culture calibrations with planktic foraminifera. *Geochimica et Cosmochimica Acta*, *193*, 197–221. <https://doi.org/10.1016/j.gca.2016.08.015>
- Anand, P., Elderfield, H., & Conte, M. H. (2003). Calibration of Mg/Ca thermometry in planktonic foraminifera from a sediment trap time series. *Paleoceanography*, *18*(2), n/a. <https://doi.org/10.1029/2002PA000846>
- Arbuszewski, J., deMenocal, P., Kaplan, A., & Farmer, E. C. (2010). On the fidelity of shell-derived $\delta^{18}\text{O}$ seawater estimates. *Earth and Planetary Science Letters*, *300*, 185–196. <https://doi.org/10.1016/j.epsl.2010.10.035>
- Arbuszewski, J. A., Cléroux, C., Bradtmiller, L., & Mix, A. (2013). Meridional shifts of the Atlantic intertropical convergence zone since the Last Glacial Maximum. *Nature Geoscience*, *6*, 959–962. <https://doi.org/10.1038/ngeo1961>
- Aurahs, R., Treis, Y., Darling, K., & Kucera, M. (2011). A revised taxonomic and phylogenetic concept for the planktonic foraminifer species *Globigerinoides ruber* based on molecular and morphometric evidence. *Marine Micropaleontology*, *79*, 1–14. <https://doi.org/10.1016/j.marmicro.2010.12.001>
- Baatsen, M., Van Hinsbergen, D. J., Heydt, A. S., Dijkstra, H. A., Sluijs, A., Abels, H. A., & Bijl, P. K. (2016). Reconstructing geographical boundary conditions for palaeoclimate modelling during the Cenozoic. *Climate of the Past*, *12*, 1635–1644. <https://doi.org/10.5194/cp-12-1635-2016>
- Barker, S., Cacho, I., Benway, H., & Tachikawa, K. (2005). Planktonic foraminiferal Mg/Ca as a proxy for past oceanic temperatures: A methodological overview and data compilation for the Last Glacial Maximum. *Quaternary Science Reviews*, *24*, 821–834. <https://doi.org/10.1016/j.quascirev.2004.07.016>
- Barker, S., Greaves, M., & Elderfield, H. (2003). A study of cleaning procedures used for foraminiferal Mg/Ca paleothermometry. *Geochemistry, Geophysics, Geosystems*, *4*(9), n/a. <https://doi.org/10.1029/2003GC000559>
- Benway, H. M., Mix, A. C., Haley, B. A., & Klinkhammer, G. P. (2006). Eastern Pacific Warm Pool paleosalinity and climate variability: 0–30 kyr. *Paleoceanography*, *21*, PA3008. <https://doi.org/10.1029/2005PA001208>
- Bereiter, B., Eggleston, S., Schmitt, J., Nehrbaas-Ahles, C., Stocker, T. F., Fischer, H., et al. (2015). Revision of the EPICA Dome C CO₂ record from 800 to 600 kyr before present. *Geophysical Research Letters*, *42*, 542–549. <https://doi.org/10.1002/2014GL061957>
- Berger, W. H. (1970). Planktonic foraminifera: Selective solution and the lysocline. *Marine Geology*, *8*(2), 111–138. [https://doi.org/10.1016/0025-3227\(70\)90001-0](https://doi.org/10.1016/0025-3227(70)90001-0)
- Bijl, P. K., Bendle, J. A., Bohaty, S. M., Pross, J., Schouten, S., Tauxe, L., et al. Expedition 318 Scientists (2013). Eocene cooling linked to early flow across the Tasmanian Gateway. *Proceedings of the National Academy of Sciences*, *110*, 9645–9650. <https://doi.org/10.1073/pnas.1220872110>
- Bijl, P. K., Schouten, S., Sluijs, A., Reichert, G.-J., Zachos, J. C., & Brinkhuis, H. (2009). Early Palaeogene temperature evolution of the southwest Pacific Ocean. *Nature*, *461*, 776–779. <https://doi.org/10.1038/nature08399>
- Boussetta, S., Kallel, N., Bassinot, F., Labeyrie, L., Duplessy, J.-C., Caillon, N., et al. (2012). Mg/Ca-paleothermometry in the western Mediterranean Sea on planktonic foraminifer species *Globigerina bulloides*: Constraints and implications. *Comptes Rendus Geoscience*, *344*, 267–276. <https://doi.org/10.1016/j.crte.2012.02.001>
- Boyer, T. P., J. I. Antonov, O. K. Baranova, C. Coleman, H. E. Garcia, A. Grodsky, et al. (2013). World ocean database 2013, Tech. rep., NOAA, Silver Spring, MD.
- Boyle, E., & Keigwin, L. (1985). Comparison of Atlantic and Pacific paleochemical records for the last 215,000 years: Changes in deep ocean circulation and chemical inventories. *Earth and Planetary Science Letters*, *76*(1-2), 135–150. [https://doi.org/10.1016/0012-821X\(85\)90154-2](https://doi.org/10.1016/0012-821X(85)90154-2)
- Brennan, S. T., Lowenstein, T. K., & Cendón, D. I. (2013). The major-ion composition of Cenozoic seawater: The past 36 million years from fluid inclusions in marine halite. *American Journal of Science*, *313*, 713–775. <https://doi.org/10.2475/08.2013.01>
- Brown, S. J., & Elderfield, H. (1996). Variations in Mg/Ca and Sr/Ca ratios of planktonic foraminifera caused by postdepositional dissolution: Evidence of shallow Mg-dependent dissolution. *Paleoceanography*, *11*(5), 543–551. <https://doi.org/10.1029/96PA01491>
- Carpenter, B., Gelman, A., Hoffman, M. D., Lee, D., Goodrich, B., Betancourt, M., et al. (2017). Stan: A probabilistic programming language. *Journal of Statistical Software*, *76*. <https://doi.org/10.18637/jss.v076.i01>
- Cléroux, C., Cortijo, E., Anand, P., Labeyrie, L., Bassinot, F., Caillon, N., & Duplessy, J.-C. (2008). Mg/Ca and Sr/Ca ratios in planktonic foraminifera: Proxies for upper water column temperature reconstruction. *Paleoceanography and Paleoclimatology*, *23*, PA3214.

- Coggon, R. M., Teagle, D. A., Smith-Duque, C. E., Alt, J. C., & Cooper, M. J. (2010). Reconstructing past seawater Mg/Ca and Sr/Ca from mid-ocean ridge flank calcium carbonate veins. *Science*, 327, 1114–1117. <https://doi.org/10.1126/science.1182252>
- Cramwinckel, M. J., Huber, M., Kocken, I. J., Agnini, C., Bijl, P. K., Bohaty, S. M., et al. (2018). Synchronous tropical and polar temperature evolution in the Eocene. *Nature*, 559, 382–386. <https://doi.org/10.1038/s41586-018-0272-2>
- Dahl, K. A., & Oppo, D. W. (2006). Sea surface temperature pattern reconstructions in the Arabian Sea. *Paleoceanography*, 21, PA1014. <https://doi.org/10.1029/2005PA001162>
- Dai, Y., Yu, J., DeMenocal, P., & Hyams-Kaphzan, O. (2019). Influences of temperature and secondary environmental parameters on planktonic foraminiferal Mg/Ca: A new core-top calibration. *Geochemistry, Geophysics, Geosystems*, 20(9), 4370–4381. <https://doi.org/10.1029/2019GC008526>
- Darling, K. F., Kucera, M., Kroon, D., & Wade, C. M. (2006). A resolution for the coiling direction paradox in *Neogloboquadrina pachyderma*. *Paleoceanography*, 21, n/a. <https://doi.org/10.1029/2005PA001189>
- Davis, C. V., Fehrenbacher, J. S., Hill, T. M., Russell, A. D., & Spero, H. J. (2017). Relationships between temperature, pH, and crusting on Mg/Ca ratios in laboratory-grown *Neogloboquadrina Foraminifera*. *Paleoceanography*, 32, 1137–1152. <https://doi.org/10.1002/2017PA003111>
- de Garidel-Thoron, T., Rosenthal, Y., Beaufort, L., Bard, E., Sonzogni, C., & Mix, A. C. (2007). A multiproxy assessment of the western equatorial Pacific hydrography during the last 30 kyr. *Paleoceanography*, 22, PA3204. <https://doi.org/10.1029/2006PA001269>
- De Nooijer, L., Van Dijk, I., Toyofuku, T., & Reichert, G. (2017). The impacts of seawater Mg/Ca and temperature on element incorporation in benthic foraminiferal calcite. *Geochemistry, Geophysics, Geosystems*, 18, 3617–3630. <https://doi.org/10.1002/2017GC007183>
- Dekens, P. S., Lea, D. W., Pak, D. K., & Spero, H. J. (2002). Core top calibration of Mg/Ca in tropical foraminifera: Refining paleotemperature estimation. *Geochemistry, Geophysics, Geosystems*, 3(4), 1–29. <https://doi.org/10.1029/2001GC000200>
- Delaney, M. L., Bé, A. W., & Boyle, E. A. (1985). Li, Sr, Mg, and Na in foraminiferal calcite shells from laboratory culture, sediment traps, and sediment cores. *Geochimica et Cosmochimica Acta*, 49(6), 1327–1341. [https://doi.org/10.1016/0016-7037\(85\)90284-4](https://doi.org/10.1016/0016-7037(85)90284-4)
- Dickson, A., & Millero, F. J. (1987). A comparison of the equilibrium constants for the dissociation of carbonic acid in seawater media. *Deep Sea Research Part A: Oceanographic Research Papers*, 34(10), 1733–1743. [https://doi.org/10.1016/0198-0149\(87\)90021-5](https://doi.org/10.1016/0198-0149(87)90021-5)
- Dickson, J. (2002). Fossil echinoderms as monitor of the Mg/Ca ratio of Phanerozoic oceans. *Science*, 298(5596), 1222–1224. <https://doi.org/10.1126/science.1075882>
- Dickson, J. (2004). Echinoderm skeletal preservation: Calcite-aragonite seas and the Mg/Ca ratio of Phanerozoic oceans. *Journal of Sedimentary Research*, 74, 355–365. <https://doi.org/10.1306/112203740355>
- Dueñas-Bohórquez, A., da Rocha, R. E., Kuroyanagi, A., Bijma, J., & Reichert, G.-J. (2009). Effect of salinity and seawater calcite saturation state on Mg and Sr incorporation in cultured planktonic foraminifera. *Marine Micropaleontology*, 73, 178–189. <https://doi.org/10.1016/j.marmicro.2009.09.002>
- Dunlea, A. G., Murray, R. W., Ramos, D. P. S., & Higgins, J. A. (2017). Cenozoic global cooling and increased seawater Mg/Ca via reduced reverse weathering. *Nature Communications*, 8, 844. <https://doi.org/10.1038/s41467-017-00853-5>
- Dyez, K. A., Zahn, R., & Hall, I. R. (2014). Multicentennial Agulhas leakage variability and links to North Atlantic climate during the past 80,000 years. *Paleoceanography*, 29, 1238–1248. <https://doi.org/10.1002/2014PA002698>
- Elderfield, H., & Ganssen, G. (2000). Past temperature and $\delta^{18}\text{O}$ of surface ocean waters inferred from foraminiferal Mg/Ca ratios. *Nature*, 405(6785), 442–445. <https://doi.org/10.1038/35013033>
- Elderfield, H., Vautravers, M., & Cooper, M. (2002). The relationship between shell size and Mg/Ca, Sr/Ca, $\delta^{18}\text{O}$, and $\delta^{13}\text{C}$ of species of planktonic foraminifera. *Geochemistry, Geophysics, Geosystems*, 3(8), 1–13. <https://doi.org/10.1029/2001GC000194>
- Erez, J., & Honjo, S. (1981). Comparison of isotopic composition of planktonic foraminifera in plankton tows, sediment traps and sediments. *Palaeogeography, Palaeoclimatology, Palaeoecology*, 33(1–3), 129–156.
- Evans, D., Brierley, C., Raymo, M. E., Erez, J., & Müller, W. (2016). Planktic foraminifera shell chemistry response to seawater chemistry: Pliocene–Pleistocene seawater Mg/Ca, temperature and sea level change. *Earth and Planetary Science Letters*, 438, 139–148. <https://doi.org/10.1016/j.epsl.2016.01.013>
- Evans, D., Erez, J., Oron, S., & Müller, W. (2015). Mg/Ca-temperature and seawater-test chemistry relationships in the shallow-dwelling large benthic foraminifera *Operculina ammonoides*. *Geochimica et Cosmochimica Acta*, 148, 325–342. <https://doi.org/10.1016/j.gca.2014.09.039>
- Evans, D., & Müller, W. (2012). Deep time foraminifera Mg/Ca paleothermometry: Nonlinear correction for secular change in seawater Mg/Ca. *Paleoceanography and Paleoclimatology*, 27.
- Evans, D., Sahoo, N., Renema, W., Cotton, L. J., Müller, W., Todd, J. A., et al. (2018). Eocene greenhouse climate revealed by coupled clumped isotope-Mg/Ca thermometry. *Proceedings of the National Academy of Sciences*, 201714744.
- Evans, D., Wade, B. S., Henehan, M., Erez, J., & Müller, W. (2016). Revisiting carbonate chemistry controls on planktic foraminifera Mg/Ca: Implications for sea surface temperature and hydrology shifts over the Paleocene–Eocene Thermal Maximum and Eocene–Oligocene transition. *Climate of the Past*, 12, 819–835. <https://doi.org/10.5194/cp-12-819-2016>
- Fairbanks, R. G., Wiebe, P. H., & Bé, A. W. (1980). Vertical distribution and isotopic composition of living planktonic foraminifera in the western North Atlantic. *Science*, 207(4426), 61–63. <https://doi.org/10.1126/science.207.4426.61>
- Fallet, U., Castañeda, I. S., Henry-Edwards, A., Richter, T. O., Boer, W., Schouten, S., & Brummer, G.-J. (2012). Sedimentation and burial of organic and inorganic temperature proxies in the Mozambique Channel, SW Indian Ocean. *Deep Sea Research Part 1: Oceanographic Research Papers*, 59, 37–53. <https://doi.org/10.1016/j.dsr.2011.10.002>
- Farmer, E. C., Demenocal, P. B., & Marchitto, T. M. (2005). Holocene and deglacial ocean temperature variability in the Benguela upwelling region: Implications for low-latitude atmospheric circulation. *Paleoceanography*, 20, PA2018. <https://doi.org/10.1029/2004PA001049>
- Ferguson, J., Henderson, G., Kucera, M., & Rickaby, R. (2008). Systematic change of foraminiferal Mg/Ca ratios across a strong salinity gradient. *Earth and Planetary Science Letters*, 265, 153–166. <https://doi.org/10.1016/j.epsl.2007.10.011>
- Filippova, A., Kienast, M., Frank, M., & Schneider, R. (2016). Alkenone paleothermometry in the North Atlantic: A review and synthesis of surface sediment data and calibrations. *Geochemistry, Geophysics, Geosystems*, 17, 1370–1382. <https://doi.org/10.1002/2015GC006106>
- Friedrich, O., Schiebel, R., Wilson, P. A., Weldeab, S., Beer, C. J., Cooper, M. J., & Fiebig, J. (2012). Influence of test size, water depth, and ecology on Mg/Ca, Sr/Ca, $\delta^{18}\text{O}$ and $\delta^{13}\text{C}$ in nine modern species of planktic foraminifers. *Earth and Planetary Science Letters*, 319, 133–145.
- Ganssen, G., & Kroon, D. (2000). The isotopic signature of planktonic foraminifera from NE Atlantic surface sediments: Implications for the reconstruction of past oceanic conditions. *Journal of the Geological Society*, 157(3), 693–699. <https://doi.org/10.1144/jgs.157.3.693>
- Gebregiorgis, D., Hathorne, E. C., Sijinkumar, A., Nath, B. N., Nürnberg, D., & Frank, M. (2016). South Asian summer monsoon variability during the last ~54 kyrs inferred from surface water salinity and river runoff proxies. *Quaternary Science Reviews*, 138, 6–15. <https://doi.org/10.1016/j.quascirev.2016.02.012>

- Gelman, A., Carlin, J., Stern, H., & Rubin, D. (2003). *Bayesian data analysis*, (2nd ed.). Boca Raton: Chapman & Hall/CRC.
- Gibbons, F. T., Oppo, D. W., Mohtadi, M., Rosenthal, Y., Cheng, J., Liu, Z., & Linsley, B. K. (2014). Deglacial $\delta^{18}\text{O}$ and hydrologic variability in the tropical Pacific and Indian Oceans. *Earth and Planetary Science Letters*, *387*, 240–251. <https://doi.org/10.1016/j.epsl.2013.11.032>
- Gothmann, A. M., Stolarski, J., Adkins, J. F., Schoene, B., Dennis, K. J., Schrag, D. P., et al. (2015). Fossil corals as an archive of secular variations in seawater chemistry since the Mesozoic. *Geochimica et Cosmochimica Acta*, *160*, 188–208. <https://doi.org/10.1016/j.gca.2015.03.018>
- Gray, W. R., & Evans, D. (2019). Non-thermal influences on Mg/Ca in planktonic foraminifera: A review of culture studies and application to the Last Glacial Maximum. *Paleoceanography and Paleoclimatology*, *34*, 306–315. <https://doi.org/10.1029/2018PA003517>
- Gray, W. R., Weldeab, S., Lea, D. W., Rosenthal, Y., Gruber, N., Donner, B., & Fischer, G. (2018). The effects of temperature, salinity, and the carbonate system on Mg/Ca in *Globigerinoides ruber* (white): A global sediment trap calibration. *Earth and Planetary Science Letters*, *482*, 607–620. <https://doi.org/10.1016/j.epsl.2017.11.026>
- Hakim, G. J., Emile-Geay, J., Steig, E. J., Noone, D., Anderson, D. M., Tardif, R., et al. (2016). The last millennium climate reanalysis project: Framework and first results. *Journal of Geophysical Research-Atmospheres*, *121*, 6745–6764. <https://doi.org/10.1002/2016JD024751>
- Hastings, D. W., Russell, A. D., & Emerson, S. R. (1998). Foraminiferal magnesium in *Globigerinoides sacculifer* as a paleotemperature proxy. *Paleoceanography and Paleoclimatology*, *13*(2), 161–169. <https://doi.org/10.1029/97PA03147>
- Hauzer, H., Evans, D., Müller, W., Rosenthal, Y., & Erez, J. (2018). Calibration of Na partitioning in the calcitic foraminifer *Operculina ammonoides* under variable Ca concentration: Toward reconstructing past seawater composition. *Earth and Planetary Science Letters*, *497*, 80–91. <https://doi.org/10.1016/j.epsl.2018.06.004>
- Herold, N., Buzan, J., Seton, M., Goldner, A., Green, J., Müller, R., et al. (2014). A suite of early Eocene (~55 Ma) climate model boundary conditions. *Geoscientific Model Development*, *7*, 2077–2090. <https://doi.org/10.5194/gmd-7-2077-2014>
- Hertzberg, J. E., & Schmidt, M. W. (2013). Refining *Globigerinoides ruber* Mg/Ca paleothermometry in the Atlantic Ocean. *Earth and Planetary Science Letters*, *383*, 123–133. <https://doi.org/10.1016/j.epsl.2013.09.044>
- Higgins, J. A., & Schrag, D. P. (2015). The Mg isotopic composition of Cenozoic seawater—Evidence for a link between Mg-clays, seawater Mg/Ca, and climate. *Earth and Planetary Science Letters*, *416*, 73–81. <https://doi.org/10.1016/j.epsl.2015.01.003>
- Hines, B. R., Hollis, C. J., Atkins, C. B., Baker, J. A., Morgans, H. E., & Strong, P. C. (2017). Reduction of oceanic temperature gradients in the early Eocene Southwest Pacific Ocean. *Palaeogeography, Palaeoclimatology, Palaeoecology*, *475*, 41–54. <https://doi.org/10.1016/j.palaeo.2017.02.037>
- Hollis, C., T. Dunkley Jones, E. Anagnostou, P. Bijl, M. Cramwinckel, Y. Cui, et al. (2019). The DeepMIP contribution to PMIP4: Methodologies for selection, compilation and analysis of latest Paleocene and early Eocene climate proxy data, incorporating version 0.1 of the DeepMIP database, Geoscientific Model Development Discussions.
- Hollis, C. J., Handley, L., Crouch, E. M., Morgans, H. E., Baker, J. A., Creech, J., et al. (2009). Tropical sea temperatures in the high-latitude South Pacific during the Eocene. *Geology*, *37*, 99–102. <https://doi.org/10.1130/G25200A.1>
- Hollis, C. J., Taylor, K. W., Handley, L., Pancost, R. D., Huber, M., Creech, J. B., et al. (2012). Early Paleogene temperature history of the Southwest Pacific Ocean: Reconciling proxies and models. *Earth and Planetary Science Letters*, *349*, 53–66.
- Hollstein, M., Mohtadi, M., Rosenthal, Y., Moffa Sanchez, P., Oppo, D., Martínez Méndez, G., et al. (2017). Stable oxygen isotopes and Mg/Ca in Planktic foraminifera from modern surface sediments of the Western Pacific Warm Pool: Implications for thermocline reconstructions. *Paleoceanography*, *32*, 1174–1194. <https://doi.org/10.1002/2017PA003122>
- Hönisch, B., Allen, K. A., Lea, D. W., Spero, H. J., Eggins, S. M., Arbuszewski, J., et al. (2013). The influence of salinity on Mg/Ca in planktic foraminifera—Evidence from cultures, core-top sediments and complementary $\delta^{18}\text{O}$. *Geochimica et Cosmochimica Acta*, *121*, 196–213. <https://doi.org/10.1016/j.gca.2013.07.028>
- Horita, J., Zimmermann, H., & Holland, H. D. (2002). Chemical evolution of seawater during the Phanerozoic: Implications from the record of marine evaporites. *Geochimica et Cosmochimica Acta*, *66*(21), 3733–3756. [https://doi.org/10.1016/S0016-7037\(01\)00884-5](https://doi.org/10.1016/S0016-7037(01)00884-5)
- Inglis, G. N., Farnsworth, A., Lunt, D., Foster, G. L., Hollis, C. J., Pagani, M., et al. (2015). Descent toward the Icehouse: Eocene sea surface cooling inferred from GDGT distributions. *Paleoceanography*, *30*, 1000–1020. <https://doi.org/10.1002/2014PA002723>
- Johnstone, H. J., Yu, J., Elderfield, H., & Schulz, M. (2011). Improving temperature estimates derived from Mg/Ca of planktonic foraminifera using X-ray computed tomography-based dissolution index, XDX. *Paleoceanography*, *26*, PA1215. <https://doi.org/10.1029/2009PA001902>
- Keigwin, L. D., Sachs, J. P., Rosenthal, Y., & Boyle, E. A. (2005). The 8200 year BP event in the slope water system, western subpolar North Atlantic. *Paleoceanography*, *20*, PA2003. <https://doi.org/10.1029/2004PA001074>
- Khider, D., Huerta, G., Jackson, C., Stott, L., & Emile-Geay, J. (2015). A Bayesian, multivariate calibration for *Globigerinoides ruber* Mg/Ca. *Geochemistry, Geophysics, Geosystems*, *16*, 2916–2932. <https://doi.org/10.1002/2015GC005844>
- Kienast, M., MacIntyre, G., Dubois, N., Higginson, S., Normandeau, C., Chazen, C., & Herbert, T. (2012). Alkenone unsaturation in surface sediments from the eastern equatorial Pacific: Implications for SST reconstructions. *Paleoceanography*, *27*, PA1210. <https://doi.org/10.1029/2011PA002254>
- Kisakürek, B., Eisenhauer, A., Böhm, F., Garbe-Schönberg, D., & Erez, J. (2008). Controls on shell Mg/Ca and Sr/Ca in cultured planktonic foraminifera, *Globigerinoides ruber* (white). *Earth and Planetary Science Letters*, *273*(3–4), 260–269. <https://doi.org/10.1016/j.epsl.2008.06.026>
- Kozdon, R., Eisenhauer, A., Weinelt, M., Meland, M. Y., & Nürnberg, D. (2009). Reassessing Mg/Ca temperature calibrations of *Neogloboquadrina pachyderma* (sinistral) using paired $\delta^{44}\text{Ca}$ and Mg/Ca measurements. *Geochemistry, Geophysics, Geosystems*, *10*, Q03005.
- Kristjánisdóttir, G. B., Moros, M., Andrews, J. T., & Jennings, A. E. (2017). Holocene Mg/Ca, alkenones, and light stable isotope measurements on the outer North Iceland shelf (MD99-2269): A comparison with other multi-proxy data and sub-division of the Holocene. *The Holocene*, *27*, 52–62. <https://doi.org/10.1177/0959683616652703>
- Kubota, Y., Kimoto, K., Tada, R., Oda, H., Yokoyama, Y., & Matsuzaki, H. (2010). Variations of East Asian summer monsoon since the last deglaciation based on Mg/Ca and oxygen isotope of planktic foraminifera in the northern East China Sea. *Paleoceanography and Paleoclimatology*, *25*, PA4205.
- Lauvset, S. K., Key, R. M., Olsen, A., van Heuven, S., Velo, A., Lin, X., et al. (2016). A new global interior ocean mapped climatology: The 1 × 1 GLODAP version 2. *Earth System Science Data*, *8*(2), 325–340. <https://doi.org/10.5194/essd-8-325-2016>
- Lea, D. W., Mashiotta, T. A., & Spero, H. J. (1999). Controls on magnesium and strontium uptake in planktonic foraminifera determined by live culturing. *Geochimica et Cosmochimica Acta*, *63*(16), 2369–2379. [https://doi.org/10.1016/S0016-7037\(99\)00197-0](https://doi.org/10.1016/S0016-7037(99)00197-0)
- Lea, D. W., Pak, D. K., Belanger, C. L., Spero, H. J., Hall, M. A., & Shackleton, N. J. (2006). Paleoclimate history of Galapagos surface waters over the last 135,000 yr. *Quaternary Science Reviews*, *25*, 1152–1167. <https://doi.org/10.1016/j.quascirev.2005.11.010>
- Lea, D. W., Pak, D. K., Peterson, L. C., & Hughen, K. A. (2003). Synchronicity of tropical and high-latitude Atlantic temperatures over the last glacial termination. *Science*, *301*(5638), 1361–1364. <https://doi.org/10.1126/science.1088470>

- Lea, D. W., Pak, D. K., & Spero, H. J. (2000). Climate impact of late Quaternary equatorial Pacific sea surface temperature variations. *Science*, 289(5485), 1719–1724. <https://doi.org/10.1126/science.289.5485.1719>
- Leduc, G., Vidal, L., Tachikawa, K., Rostek, F., Sonzogni, C., Beaufort, L., & Bard, E. (2007). Moisture transport across Central America as a positive feedback on abrupt climatic changes. *Nature*, 445, 908–911. <https://doi.org/10.1038/nature05578>
- Levi, C., Labeyrie, L., Bassinot, F., Guichard, F., Cortijo, E., Waelbroeck, C., et al. (2007). Low-latitude hydrological cycle and rapid climate changes during the last deglaciation. *Geochemistry, Geophysics, Geosystems*, 8, Q05N12.
- Linsley, B. K., Rosenthal, Y., & Oppo, D. W. (2010). Holocene evolution of the Indonesian throughflow and the western Pacific warm pool. *Nature Geoscience*, 3, 578–583. <https://doi.org/10.1038/ngeo920>
- Lombard, F., Labeyrie, L., Michel, E., Bopp, L., Cortijo, E., Retaillieu, S., et al. (2011). Modelling planktic foraminifer growth and distribution using an ecophysiological multi-species approach. *Biogeosciences*, 8, 853–873. <https://doi.org/10.5194/bg-8-853-2011>
- Lombard, F., Labeyrie, L., Michel, E., Spero, H. J., & Lea, D. W. (2009). Modelling the temperature dependent growth rates of planktic foraminifera. *Marine Micropaleontology*, 70, 1–7. <https://doi.org/10.1016/j.marmicro.2008.09.004>
- Lowenstein, T. K., Timofeeff, M. N., Brennan, S. T., Hardie, L. A., & Demicco, R. V. (2001). Oscillations in Phanerozoic seawater chemistry: Evidence from fluid inclusions. *Science*, 294(5544), 1086–1088. <https://doi.org/10.1126/science.1064280>
- Malevich, S., Vetter, L., & Tierney, J. (2019). Global core top calibration of $\delta^{18}\text{O}$ in planktic foraminifera to sea-surface temperature. *Paleoceanography*, 34, 1292–1315. <https://doi.org/10.1029/2019PA003576>
- Marchitto, T. M., Muscheler, R., Ortiz, J. D., Carriquiry, J. D., & van Geen, A. (2010). Dynamical response of the tropical Pacific Ocean to solar forcing during the early Holocene. *Science*, 330, 1378–1381. <https://doi.org/10.1126/science.1194887>
- Mashiotta, T. A., Lea, D. W., & Spero, H. J. (1999). Glacial–interglacial changes in Subantarctic sea surface temperature and $\delta^{18}\text{O}$ -water using foraminiferal Mg. *Earth and Planetary Science Letters*, 170(4), 417–432. [https://doi.org/10.1016/S0012-821X\(99\)00116-8](https://doi.org/10.1016/S0012-821X(99)00116-8)
- Mathien-Blard, E., & Bassinot, F. (2009). Salinity bias on the foraminifera Mg/Ca thermometry: Correction procedure and implications for past ocean hydrographic reconstructions. *Geochemistry, Geophysics, Geosystems*, 10, n/a. <https://doi.org/10.1029/2008GC002353>
- McConnell, M. C., & Thunell, R. C. (2005). Calibration of the planktonic foraminiferal Mg/Ca paleothermometer: Sediment trap results from the Guaymas Basin, Gulf of California. *Paleoceanography and Paleoclimatology*, 20.
- Meland, M. Y., Jansen, E., Elderfield, H., Dokken, T. M., Olsen, A., & Bellerby, R. G. (2006). Mg/Ca ratios in the planktonic foraminifer *Neoglobobulimina pachyderma* (sinistral) in the northern North Atlantic/Nordic Seas. *Geochemistry, Geophysics, Geosystems*, 7, Q06P14.
- Mewes, A., Langer, G., de Nooijer, L. J., Bijma, J., & Reichert, G.-J. (2014). Effect of different seawater Mg^{2+} concentrations on calcification in two benthic foraminifera. *Marine Micropaleontology*, 113, 56–64. <https://doi.org/10.1016/j.marmicro.2014.09.003>
- Moffa-Sánchez, P., Hall, I. R., Barker, S., Thornalley, D. J., & Yashayaev, I. (2014). Surface changes in the eastern Labrador Sea around the onset of the Little Ice Age. *Paleoceanography*, 29, 160–175. <https://doi.org/10.1002/2013PA002523>
- Mohtadi, M., Oppo, D. W., Lückge, A., DePol-Holz, R., Steinke, S., Groeneveld, J., et al. (2011). Reconstructing the thermal structure of the upper ocean: Insights from planktic foraminifera shell chemistry and alkenones in modern sediments of the tropical eastern Indian Ocean. *Paleoceanography and Paleoclimatology*, 26, PA3219.
- Mohtadi, M., Steinke, S., Groeneveld, J., Fink, H. G., Rixen, T., Hebbeln, D., et al. (2009). Low-latitude control on seasonal and interannual changes in planktonic foraminiferal flux and shell geochemistry off south Java: A sediment trap study. *Paleoceanography*, 24, n/a. <https://doi.org/10.1029/2008PA001636>
- Mohtadi, M., Steinke, S., Lückge, A., Groeneveld, J., & Hathorne, E. C. (2010). Glacial to Holocene surface hydrography of the tropical eastern Indian Ocean. *Earth and Planetary Science Letters*, 292, 89–97. <https://doi.org/10.1016/j.epsl.2010.01.024>
- Morley, A., Babila, T. L., Wright, J., Ninnemann, U., Kleiven, K., Irvail, N., & Rosenthal, Y. (2017). Environmental controls on Mg/Ca in *Neoglobobulimina incompta*: A core-top study from the subpolar North Atlantic. *Geochemistry, Geophysics, Geosystems*, 18, 4276–4298. <https://doi.org/10.1002/2017GC007111>
- Mortyn, P. G., & Charles, C. D. (2003). Planktonic foraminiferal depth habitat and $\delta^{18}\text{O}$ calibrations: Plankton tow results from the Atlantic sector of the Southern Ocean. *Paleoceanography*, 18(2), n/a. <https://doi.org/10.1029/2001PA000637>
- Mucci, A., & Morse, J. W. (1983). The incorporation of Mg^{2+} and Sr^{2+} into calcite overgrowths: Influences of growth rate and solution composition. *Geochimica et Cosmochimica Acta*, 47(2), 217–233. [https://doi.org/10.1016/0016-7037\(83\)90135-7](https://doi.org/10.1016/0016-7037(83)90135-7)
- Nürnberg, D., Bijma, J., & Hemleben, C. (1996). Assessing the reliability of magnesium in foraminiferal calcite as a proxy for water mass temperatures. *Geochimica et Cosmochimica Acta*, 60(5), 803–814. [https://doi.org/10.1016/0016-7037\(95\)00446-7](https://doi.org/10.1016/0016-7037(95)00446-7)
- Nürnberg, D., Ziegler, M., Karas, C., Tiedemann, R., & Schmidt, M. W. (2008). Interacting Loop Current variability and Mississippi River discharge over the past 400 kyr. *Earth and Planetary Science Letters*, 272, 278–289. <https://doi.org/10.1016/j.epsl.2008.04.051>
- O'Brien, C. L., Foster, G. L., Martínez-Botí, M. A., Abell, R., Rae, J. W., & Pancost, R. D. (2014). High sea surface temperatures in tropical warm pools during the Pliocene. *Nature Geoscience*, 7, 606–611. <https://doi.org/10.1038/ngeo2194>
- Oomori, T., Kaneshima, H., Maezato, Y., & Kitano, Y. (1987). Distribution coefficient of Mg^{2+} ions between calcite and solution at 10–50°C. *Marine Chemistry*, 20(4), 327–336. [https://doi.org/10.1016/0304-4203\(87\)90066-1](https://doi.org/10.1016/0304-4203(87)90066-1)
- Oppo, D. W., Rosenthal, Y., & Linsley, B. K. (2009). 2,000-year-long temperature and hydrology reconstructions from the Indo-Pacific warm pool. *Nature*, 460(7259), 1113–1116. <https://doi.org/10.1038/nature08233>
- Oppo, D. W., & Sun, Y. (2005). Amplitude and timing of sea-surface temperature change in the northern South China Sea: Dynamic link to the East Asian monsoon. *Geology*, 33, 785–788. <https://doi.org/10.1130/G21867.1>
- Pahnke, K., Zahn, R., Elderfield, H., & Schulz, M. (2003). 340,000-year centennial-scale marine record of Southern Hemisphere climatic oscillation. *Science*, 301(5635), 948–952. <https://doi.org/10.1126/science.1084451>
- Palmer, M., & Pearson, P. N. (2003). A 23,000-year record of surface water pH and pCO_2 in the western equatorial Pacific Ocean. *Science*, 300(5618), 480–482. <https://doi.org/10.1126/science.1080796>
- Parker, A. O., Schmidt, M. W., Jobe, Z. R., & Slowey, N. C. (2016). A new perspective on West African hydroclimate during the last deglaciation. *Earth and Planetary Science Letters*, 449, 79–88. <https://doi.org/10.1016/j.epsl.2016.05.038>
- Pearson, P. N., van Dongen, B. E., Nicholas, C. J., Pancost, R. D., Schouten, S., Singano, J. M., & Wade, B. S. (2007). Stable warm tropical climate through the Eocene Epoch. *Geology*, 35, 211–214. <https://doi.org/10.1130/G23175A.1>
- van Raden, U. J., Groeneveld, J., Raitzsch, M., & Kucera, M. (2011). Mg/Ca in the planktonic foraminifera *Globorotalia inflata* and *Globigerinoides bulloides* from Western Mediterranean plankton tow and core top samples. *Marine Micropaleontology*, 78, 101–112. <https://doi.org/10.1016/j.marmicro.2010.11.002>
- Raitzsch, M., Dueñas-Bohórquez, A., Reichert, G.-J., de Nooijer, L. J., & Bickert, T. (2010). Incorporation of Mg and Sr in calcite of cultured benthic foraminifera: Impact of calcium concentration and associated calcite saturation state. *Biogeosciences*, 7, 869–881. <https://doi.org/10.5194/bg-7-869-2010>
- Ravelo, A., & Fairbanks, R. (1992). Oxygen isotopic composition of multiple species of planktonic foraminifera: Recorders of the modern photic zone temperature gradient. *Paleoceanography and Paleoclimatology*, 7(6), 815–831. <https://doi.org/10.1029/92PA02092>

- Regenberg, M., Nürnberg, D., Steph, S., Groeneveld, J., Garbe-Schönberg, D., Tiedemann, R., & Dullo, W.-C. (2006). Assessing the effect of dissolution on planktonic foraminiferal Mg/Ca ratios: Evidence from Caribbean core tops. *Geochemistry, Geophysics, Geosystems*, 7, n/a. <https://doi.org/10.1029/2005GC001019>
- Regenberg, M., Regenberg, A., Garbe-Schönberg, D., & Lea, D. W. (2014). Global dissolution effects on planktonic foraminiferal Mg/Ca ratios controlled by the calcite-saturation state of bottom waters. *Paleoceanography*, 29, 127–142. <https://doi.org/10.1002/2013PA002492>
- Regenberg, M., Steph, S., Nürnberg, D., Tiedemann, R., & Garbe-Schönberg, D. (2009). Calibrating Mg/Ca ratios of multiple planktonic foraminiferal species with $\delta^{18}\text{O}$ -calcification temperatures: Paleothermometry for the upper water column. *Earth and Planetary Science Letters*, 278, 324–336. <https://doi.org/10.1016/j.epsl.2008.12.019>
- Reynolds, L. A., & Thunell, R. C. (1986). Seasonal production and morphologic variation of *Neogloboquadrina pachyderma* (Ehrenberg) in the northeast Pacific. *Micropaleontology*, 32(1), 1–18. <https://doi.org/10.2307/1485696>
- Richey, J. N., Poore, R. Z., Flower, B. P., & Hollander, D. J. (2012). Ecological controls on the shell geochemistry of pink and white *Globigerinoides ruber* in the northern Gulf of Mexico: Implications for paleoceanographic reconstruction. *Marine Micropaleontology*, 82–83, 28–37. <https://doi.org/10.1016/j.marmicro.2011.10.002>
- Richey, J. N., Poore, R. Z., Flower, B. P., & Quinn, T. M. (2007). 1400 yr multiproxy record of climate variability from the northern Gulf of Mexico. *Geology*, 35, 423–426. <https://doi.org/10.1130/G23507A.1>
- Richey, J. N., Poore, R. Z., Flower, B. P., Quinn, T. M., & Hollander, D. J. (2009). Regionally coherent Little Ice Age cooling in the Atlantic warm pool. *Geophysical Research Letters*, 36, L21703. <https://doi.org/10.1029/2009GL040445>
- Richey, J. N., Thirumalai, K., Khider, D., Reynolds, C. E., Partin, J. W., & Quinn, T. M. (2019). Considerations for *Globigerinoides ruber* (White and Pink) paleoceanography: Comprehensive insights from a long-running sediment trap. *Paleoceanography and Paleoclimatology*, 34, 353–373. <https://doi.org/10.1029/2018PA003417>
- Rietthorff, J.-R., Max, L., Nürnberg, D., Lembke-Jene, L., & Tiedemann, R. (2013). Deglacial development of (sub) sea surface temperature and salinity in the subarctic northwest Pacific: Implications for upper-ocean stratification. *Paleoceanography*, 28, 91–104. <https://doi.org/10.1002/palo.20014>
- Romahn, S., Mackensen, A., Groeneveld, J., & Pätzold, J. (2014). Deglacial intermediate water reorganization: New evidence from the Indian Ocean. *Climate of the Past*, 10, 293–303. <https://doi.org/10.5194/cp-10-293-2014>
- Rosenthal, Y., & Boyle, E. A. (1993). Factors controlling the fluoride content of planktonic foraminifera: An evaluation of its paleoceanographic applicability. *Geochimica et Cosmochimica Acta*, 57(2), 335–346. [https://doi.org/10.1016/0016-7037\(93\)90435-Y](https://doi.org/10.1016/0016-7037(93)90435-Y)
- Rosenthal, Y., Lohmann, G., Lohmann, K., & Sherrell, R. (2000). Incorporation and preservation of Mg in *Globigerinoides sacculifer*: Implications for reconstructing the temperature and $^{18}\text{O}/^{16}\text{O}$ of seawater. *Paleoceanography*, 15(1), 135–145. <https://doi.org/10.1029/1999PA000415>
- Rosenthal, Y., & Lohmann, G. P. (2002). Accurate estimation of sea surface temperatures using dissolution-corrected calibrations for Mg/Ca paleothermometry. *Paleoceanography*, 17(3), 16–16-6. <https://doi.org/10.1029/2001PA000749>
- Rosenthal, Y., Oppo, D. W., & Linsley, B. K. (2003). The amplitude and phasing of climate change during the last deglaciation in the Sulu Sea, western equatorial Pacific. *Geophysical Research Letters*, 30(8). <https://doi.org/10.1029/2002GL016612>
- Rosenthal, Y., Perron-Cashman, S., Lear, C. H., Bard, E., Barker, S., Billups, K., et al. (2004). Interlaboratory comparison study of Mg/Ca and Sr/Ca measurements in planktonic foraminifera for paleoceanographic research. *Geochemistry, Geophysics, Geosystems*, 5, n/a. <https://doi.org/10.1029/2003GC000650>
- Russell, A. D., Emerson, S., Nelson, B. K., Erez, J., & Lea, D. W. (1994). Uranium in foraminiferal calcite as a recorder of seawater uranium concentrations. *Geochimica et Cosmochimica Acta*, 58(2), 671–681. [https://doi.org/10.1016/0016-7037\(94\)90497-9](https://doi.org/10.1016/0016-7037(94)90497-9)
- Russell, A. D., Hönisch, B., Spero, H. J., & Lea, D. W. (2004). Effects of seawater carbonate ion concentration and temperature on shell U, Mg, and Sr in cultured planktonic foraminifera. *Geochimica et Cosmochimica Acta*, 68, 4347–4361. <https://doi.org/10.1016/j.gca.2004.03.013>
- Rustic, G. T., Koutavas, A., Marchitto, T. M., & Linsley, B. K. (2015). Dynamical excitation of the tropical Pacific Ocean and ENSO variability by Little Ice Age cooling. *Science*, 350(6267), 1537–1541. <https://doi.org/10.1126/science.aac9937>
- Sabbatini, A., Bassinot, F., Boussetta, S., Negri, A., Rebaubier, H., Dewilde, F., et al. (2011). Further constraints on the diagenetic influences and salinity effect on *Globigerinoides ruber* (white) Mg/Ca thermometry: Implications in the Mediterranean Sea. *Geochemistry, Geophysics, Geosystems*, 12, n/a. <https://doi.org/10.1029/2011GC003675>
- Sadekov, A. Y., Darling, K. F., Ishimura, T., Wade, C. M., Kimoto, K., Singh, A. D., et al. (2016). Geochemical imprints of genotypic variants of *Globigerina bulloides* in the Arabian Sea. *Paleoceanography*, 31, 1440–1452. <https://doi.org/10.1002/2016PA002947>
- Saenger, C. P., & Evans, M. N. (2019). Calibration and validation of environmental controls on planktic foraminifera Mg/Ca using global coretop data. *Paleoceanography and Paleoclimatology*, 34, 1249–1270. <https://doi.org/10.1029/2018PA003507>
- Saraswat, R., Lea, D. W., Nigam, R., Mackensen, A., & Naik, D. K. (2013). Deglaciation in the tropical Indian Ocean driven by interplay between the regional monsoon and global teleconnections. *Earth and Planetary Science Letters*, 375, 166–175. <https://doi.org/10.1016/j.epsl.2013.05.022>
- Schmidt, M. W., Chang, P., Hertzberg, J. E., Them, T. R., Ji, L., & Otto-Bliesner, B. L. (2012). Impact of abrupt deglacial climate change on tropical Atlantic subsurface temperatures. *Proceedings of the National Academy of Science*, 109, 14,348–14,352. <https://doi.org/10.1073/pnas.1207806109>
- Schmidt, M. W., Spero, H. J., & Lea, D. W. (2004). Links between salinity variation in the Caribbean and North Atlantic thermohaline circulation. *Nature*, 428, 160–163. <https://doi.org/10.1038/nature02346>
- Schmidt, M. W., Weinlein, W. A., Marcantonio, F., & Lynch-Stieglitz, J. (2012). Solar forcing of Florida Straits surface salinity during the early Holocene. *Paleoceanography*, 27, PA3204. <https://doi.org/10.1029/2012PA002284>
- Segev, E., & Erez, J. (2006). Effect of Mg/Ca ratio in seawater on shell composition in shallow benthic foraminifera. *Geochemistry, Geophysics, Geosystems*, 7, Q02P09.
- Sjöberg, E. (1976). A fundamental equation for calcite dissolution kinetics. *Geochimica et Cosmochimica Acta*, 40, 441–447. [https://doi.org/10.1016/0016-7037\(76\)90009-0](https://doi.org/10.1016/0016-7037(76)90009-0)
- Steinke, S., Chiu, H.-Y., Yu, P.-S., Shen, C.-C., Löwemark, L., Mii, H.-S., & Chen, M.-T. (2005). Mg/Ca ratios of two *Globigerinoides ruber* (white) morphotypes: Implications for reconstructing past tropical/subtropical surface water conditions. *Geochemistry, Geophysics, Geosystems*, 6, Q11005.
- Steinke, S., Kienast, M., Groeneveld, J., Lin, L.-C., Chen, M.-T., & Rendle-Bühning, R. (2008). Proxy dependence of the temporal pattern of deglacial warming in the tropical South China Sea: Toward resolving seasonality. *Quaternary Science Reviews*, 27, 688–700. <https://doi.org/10.1016/j.quascirev.2007.12.003>
- Stott, L., Timmermann, A., & Thunell, R. (2007). Southern Hemisphere and deep-sea warming led deglacial atmospheric CO₂ rise and tropical warming. *Science*, 318, 435–438. <https://doi.org/10.1126/science.1143791>

- Sun, Y., Oppo, D. W., Xiang, R., Liu, W., & Gao, S. (2005). Last deglaciation in the Okinawa Trough: Subtropical northwest Pacific link to Northern Hemisphere and tropical climate. *Paleoceanography*, *20*, PA4005. <https://doi.org/10.1029/2004PA001061>
- Taylor, B. J., Rae, J. W., Gray, W. R., Darling, K. F., Burke, A., Gersonde, R., et al. (2018). Distribution and ecology of planktic foraminifera in the North Pacific: Implications for paleo-reconstructions. *Quaternary Science Reviews*, *191*, 256–274. <https://doi.org/10.1016/j.quascirev.2018.05.006>
- Thirumalai, K., Quinn, T. M., & Marino, G. (2016). Constraining past seawater $\delta^{18}\text{O}$ and temperature records developed from foraminiferal geochemistry. *Paleoceanography*, *31*, 1409–1422. <https://doi.org/10.1002/2016PA002970>
- Thornalley, D. J., Elderfield, H., & McCave, I. N. (2011). Reconstructing North Atlantic deglacial surface hydrography and its link to the Atlantic overturning circulation. *Global and Planetary Change*, *79*, 163–175. <https://doi.org/10.1016/j.gloplacha.2010.06.003>
- Tierney, J. E., Pausata, F. S., & deMenocal, P. (2016). Deglacial Indian monsoon failure and North Atlantic stadials linked by Indian Ocean surface cooling. *Nature Geoscience*, *9*, 46–50. <https://doi.org/10.1038/ngeo2603>
- Tierney, J. E., & Tingley, M. P. (2014). A Bayesian, spatially-varying calibration model for the TEX₈₆ proxy. *Geochimica et Cosmochimica Acta*, *127*, 83–106. <https://doi.org/10.1016/j.gca.2013.11.026>
- Tierney, J. E., & Tingley, M. P. (2018). BAYSPLINE: A new calibration for the alkenone paleothermometer. *Paleoceanography and Paleoclimatology*, *33*, 281–301. <https://doi.org/10.1002/2017PA003201>
- Timmermann, A., Sachs, J., & Timm, O. E. (2014). Assessing divergent SST behavior during the last 21 ka derived from alkenones and *G. ruber*-Mg/Ca in the equatorial Pacific. *Paleoceanography*, *29*, 680–696. <https://doi.org/10.1002/2013PA002598>
- Tripathi, A. K., Delaney, M. L., Zachos, J. C., Anderson, L. D., Kelly, D. C., & Elderfield, H. (2003). Tropical sea-surface temperature reconstruction for the early Paleogene using Mg/Ca ratios of planktonic foraminifera. *Paleoceanography*, *18*(4), 1101. <https://doi.org/10.1029/2003PA000937>
- Tyrrell, T., & Zeebe, R. E. (2004). History of carbonate ion concentration over the last 100 million years. *Geochimica et Cosmochimica Acta*, *68*, 3521–3530. <https://doi.org/10.1016/j.gca.2004.02.018>
- Van Heuven, S., D. Pierrot, J. Rae, E. Lewis, and D. Wallace (2011), Matlab program developed for CO₂ system calculations, ORNL/CDIAC-105b. Carbon Dioxide Information Analysis Center, Oak Ridge National Laboratory, US Department of Energy, Oak Ridge, Tennessee, 530.
- Vázquez Riveiros, N., Govin, A., Waelbroeck, C., Mackensen, A., Michel, E., Moreira, S., et al. (2016). Mg/Ca thermometry in planktic foraminifera: Improving paleotemperature estimations for *G. bulloides* and *N. pachyderma* left. *Geochemistry, Geophysics, Geosystems*, *17*, 1249–1264. <https://doi.org/10.1002/2015GC006234>
- Vehtari, A., Gelman, A., & Gabry, J. (2017). Practical Bayesian model evaluation using leave-one-out cross-validation and WAIC. *Statistics and Computing*, *27*, 1413–1432. <https://doi.org/10.1007/s11222-016-9696-4>
- Visser, K., Thunell, R., & Stott, L. (2003). Magnitude and timing of temperature change in the Indo-Pacific warm pool during deglaciation. *Nature*, *421*(6919), 152–155. <https://doi.org/10.1038/nature01297>
- Von Langen, P. J., Pak, D. K., Spero, H. J., & Lea, D. W. (2005). Effects of temperature on Mg/Ca in neogloboquadrinid shells determined by live culturing. *Geochemistry, Geophysics, Geosystems*, *6*.
- Wara, M. W., Ravelo, A. C., & Delaney, M. L. (2005). Permanent El Niño-like conditions during the Pliocene warm period. *Science*, *309*, 758–761. <https://doi.org/10.1126/science.1112596>
- Wei, G., Deng, W., Liu, Y., & Li, X. (2007). High-resolution sea surface temperature records derived from foraminiferal Mg/Ca ratios during the last 260 ka in the northern South China Sea. *Palaeogeography, Palaeoclimatology, Palaeoecology*, *250*, 126–138. <https://doi.org/10.1016/j.palaeo.2007.03.005>
- Weldeab, S., Lea, D. W., Oberhänsli, H., & Schneider, R. R. (2014). Links between southwestern tropical Indian Ocean SST and precipitation over southeastern Africa over the last 17 kyr. *Palaeogeography, Palaeoclimatology, Palaeoecology*, *410*, 200–212. <https://doi.org/10.1016/j.palaeo.2014.06.001>
- Weldeab, S., Lea, D. W., Schneider, R. R., & Andersen, N. (2007). 155,000 years of West African monsoon and ocean thermal evolution. *Science*, *316*, 1303–1307. <https://doi.org/10.1126/science.1140461>
- Weldeab, S., Schneider, R., & Kölling, M. (2006). Deglacial sea surface temperature and salinity increase in the western tropical Atlantic in synchrony with high latitude climate instabilities. *Earth and Planetary Science Letters*, *241*, 699–706. <https://doi.org/10.1016/j.epsl.2005.11.012>
- Weldeab, S., Schneider, R. R., Kölling, M., & Wefer, G. (2005). Holocene African droughts relate to eastern equatorial Atlantic cooling. *Geology*, *33*, 981–984. <https://doi.org/10.1130/G21874.1>
- Xu, J., Kuhnt, W., Holbourn, A., Regenberg, M., & Andersen, N. (2010). Indo-Pacific warm pool variability during the Holocene and Last Glacial Maximum. *Paleoceanography*, *25*, PA4230. <https://doi.org/10.1029/2010PA001934>
- Yu, J., Elderfield, H., Jin, Z., & Booth, L. (2008). A strong temperature effect on U/Ca in planktonic foraminiferal carbonates. *Geochimica et Cosmochimica Acta*, *72*, 4988–5000. <https://doi.org/10.1016/j.gca.2008.07.011>
- Zarić, S., Donner, B., Fischer, G., Mulitza, S., & Wefer, G. (2005). Sensitivity of planktic foraminifera to sea surface temperature and export production as derived from sediment trap data. *Marine Micropaleontology*, *55*, 75–105. <https://doi.org/10.1016/j.marmicro.2005.01.002>
- Zhang, Y. G., Pagani, M., & Liu, Z. (2014). A 12-million-year temperature history of the tropical Pacific Ocean. *Science*, *344*, 84–87. <https://doi.org/10.1126/science.1246172>
- Zhu, J., Poulsen, C. J., & Tierney, J. E. (2019). Simulation of Eocene extreme warmth and high climate sensitivity through cloud feedbacks. *Science Advances*, *5*, eaax1874. <https://doi.org/10.1126/sciadv.aax1874>